IPST Technical Paper Series Number 550

Macroscopic Flow Structures in a Bubbling Paper Pulp-Water Slurry

J.D. Lindsay, S.M. Ghiaasiaan, and S.I. Abdel-Khalik

January 1995

Submitted to
Industrial & Engineering Chemistry Research

MACROSCOPIC FLOW STRUCTURES IN A BUBBLING PAPER PULP-WATER SLURRY

Jeffrey D. Lindsay[1]*

Institute of Paper Science and Technology

500 10th St., NW, Atlanta, GA 30318

S. Mostafa Ghiaasiaan, and S. I. Abdel-Khalik

George W. Woodruf School of Mechanical Engineering

Georgia Institute of Technology, Atlanta, GA 30332-0405

ABSTRACT

The hydrodynamic characteristics of three-phase slurry columns containing water, paper fibers, and air have been experimentally investigated. Such systems are relevant to flotation deinking, a critical but poorly understood separation process in the production of recycled paper.

Air flow through quiescent liquids or slurries was studied with a vertical transparent test column. Three similar test series were performed using pure water, and water pulp mixtures with 1% and 2% consistency (fiber weight percent). Void fraction profiles were obtained using gamma densitometry. Flow patterns in the pulp suspensions were significantly different than those in pure water and those reported in the literature for non-fibrous three-phase columns. Fiber flocculation and network formation impede bubble motion, altering bubble size distributions and promoting early transition to unfavorable flow regimes.

A vertical cocurrent flow system was also studied in which air and pulp suspensions or water could flow simultaneously. The data indicate that gas holdup

[1] Presently at Kimberly-Clark Corp., 2100 Winchester Road, Neenah WI 54956

can increase as pulp superficial velocity is increased, due to a decrease in bubble aggregation. Bubbles that are hindered by the pulp network structure can be carried away by the bulk flow before other bubbles collide and aggregate with the impeded bubbles. As a result, there are fewer large bubbles that break through the network structure to escape with a small dwell time.

The effect of the fibers and fiber flocs on the hydrodynamics, along with potential applications for improved deinking performance, are discussed.

INTRODUCTION

While many three-phase flow systems have been studied, little basic work has been conducted with flotation deinking of recycled paper fibers, a three-phase system of significant economic importance. In flotation deinking, air bubbles are used to remove hydrophobic ink particles from an aqueous suspension of paper fibers. Flotation deinking is well suited for removing ink particles in the size range of roughly 10 to 100 μm, which is a heavily populated size range for many inks following typical pulping processes. The flotation process is becoming the backbone of many modern recycling operations.

In the late 1960s, froth flotation systems from the mineral industry were adopted by the paper industry for recycled paper deinking. Early systems had low efficiency. A number of design changes were required due to significant differences in process objectives, rheology, and surface chemistry. Modern flotation deinking cells are significantly different from the mineral systems from which they evolved. Modern deinking systems cover a wide spectrum of approaches, including venturi injection of air in open or closed tanks, dissolved air nucleation in pressurized horizontal flow cells, gas sparged cyclones with air injection through porous walls, and turbine systems in which a horizontal rotor in a large rectangular tank disperses

air into the pulp. In spite of the wide variation in designs, several common features can be found. A flotation deinking system begins with a mixing zone where a fast-moving fiber suspension is mixed with air. In the turbulent mixing zone, bubbles and ink particles collide and attach, often with the help of chemical agents such as calcium soap. Pipe Reynolds numbers (where applicable) in the mixing zone may exceed $1x10^5$. Following attachment of particles to the bubbles, the bubbles must be separated from the fiber slurry. Bubble coalescence is needed to achieve bubble size large enough to rise through the slurry. The bubbles carry the ink to the slurry surface where steady removal of the ink-laden froth may be achieved by skimming or overflow.

Most flotation deinking cells operate with a gas superficial velocity below 2 cm/s (Floccia, 1994). The volumetric flow rate of gas is typically 20-40% of the slurry flow rate, though turbine cells may achieve air to slurry flow ratios of up to 1000% and a gas superficial velocity of nearly 4 cm/s (Gilkey and Yoshida, 1992). Typical cells operate with a void volume on the order of 10-20%. Slurry retention time is on the order of 5 to 20 minutes in many systems.

Most of the development of flotation deinking for the pulp and paper industry has relied on purely empirical methods. Some manufacturers have applied flow visualization of their systems using pure water and air to gain insight into hydrodynamics and bubble size distributions, but the effect of paper fibers (which make the slurry opaque) on the hydrodynamics has been largely unexplored.

Part of the problem is the complex rheology of even "simple" two-phase pulp suspensions. The interaction of the long (ca. 1-3 mm) and thin (ca. 20-40 μm) fibers leads to unusual non-Newtonian behavior (Bird et al., 1960; Duffy et al., 1976; Lee and Duffy, 1976), even in dilute suspensions. The addition of a third phase, air, is expected to increase the complexity of the system.

RELATED WORK

On a microscopic scale, the liquid-fiber-bubble-ink particle interactions can be very complicated. Such interactions, nevertheless, are expected to be strongly influenced by the flow field hydrodynamics. The hydrodynamic attributes crucial to the performance of flotation deinking systems include:

1. Gas volume fraction and its distribution
2. Bubble size characteristics
3. Macroscopic flow field characteristics (bubble rise path, recirculation, channeling, etc.)

All these parameters have been extensively studied in the past in relation to two-and three-phase bubble columns and fluidized beds. Despite some similarities, however, the hydrodynamic characteristics of bubble columns and fluidized beds have limited applicability to fibrous pulp suspensions, as will be explained below. Below, we address primarily the literature dealing with air-water vertical columns without a throughput of water, which is relevant to much of the present study. For the low superficial velocities of pulp suspensions in this study and in general flotation deinking, studies of fluidized beds or other typical throughflow systems are usually of little value. A few relevant studies of multiphase effects in fiber suspensions are also discussed.

Two-phase, Nonfibrous Systems

Three major flow regimes have been identified in two-phase bubble columns (Shah et al., 1982; Shenderov and Dilman, 1989) There is disagreement about conditions leading to switching from one regime to another, however, and these conditions may vary with system parameters. The bubbly regime is usually assumed to occur when the superficial gas velocity, j_G, is less than 5 cm/s, and is characterized by dispersed bubbles ascending in roughly rectilinear paths, without

significant interaction among themselves. Bubbles increasingly interact with each other and coalesce for 5 cm/s $\leq j_G \leq$ 10 cm/s, eventually leading to the establishment of the churn-turbulent regime for $j_G >$ 10 cm/s if column diameter, D_c, exceeds roughly 15 cm. In the latter regime large irregular-shaped bubbles, occasionally made of globules of smaller bubbles, account for most of the gas transport in the pool (Shah et al., 1982; Godbole et al., 1982; Shah et al., 1985; Shenderov and Dilman 1989). In columns with $D_c <$ roughly 15 cm, furthermore, a slug flow may develop instead of the churn-turbulent regime, where Taylor bubbles with diameters nearly equal to the column diameter dominate the flow field (one study, Ellis and Jones, 1965, suggests the critical column diameter may be closer to 7.5 cm). The aforementioned flow regimes are based on macroscopic, time-averaged measurements.

Gross recirculation is characteristic of dispersed and coalesced vertical two-phase gas-liquid column flow (Walter et al., 1983; Ulbrecht et al., 1985), analogous to the recirculation that is established in buoyant cells. In two-phase column flow, the upward flowing gas drags along liquid, which then descends after the gas is released near the top of the column. The result is a flow pattern with ascending flow at the center of the column and descending liquid near the column wall, with an inversion point near 0.5 to 0.7R. A strong gradient in gas holdup is also established, with elevated holdup near the center of the column. Ulbrecht et al. (1985) identify three patterns for the central plume and the accompanying recirculation field: the viscous mode, helical flow mode, and vortex mode. Chen et al. (1994) have provided further insight into gross features of such flows, noting the existence of a complicated vortical-spiral central bubble stream in the bubbly-turbulent transition region.

Gas hold-up (void fraction) is a crucial parameter in bubble columns since a high void fraction implies larger total interfacial area and/or longer bubble

residence time in the pool, both of which lead to higher volumetric transfer rates. Since the column wall effect becomes weak in large diameter columns supporting a churn-turbulent regime, the gas void fraction data may be extrapolated to much larger geometries from data obtained with small scale experiments, as long as D_c>15 cm (Shah et al., 1982). Many empirical correlations have thus been proposed (Akita and Yoshida, 1973; Bach and Pilhofer, 1978; Kumar et al., 1976; Hikita et al., 1980). The drift flux model (DFM) can also be applied (Wallis, 1969; Govier and Aziz, 1972). Bubble dynamics in bubble columns operating in the churn-turbulent regime are often simplified by dividing the bubbles into two size groups, large and small (Vermeer and Krishna, 1981; Godbole et al., 1982; Shah et al., 1985, Shenderov and Dilman, 1989). Bubble rise velocities for these two bubble groups have been measured using the dynamic gas disengagement technique by several investigators (Sriram and Mann, 1977; Vermeer and Krishna, 1981; Godbole et al., 1982; Shah et al., 1985; Shenderov and Dilman, 1989).

The relationship between holdup and gas flux often depends on details of gas injection. This was illustrated in the work of Zuber and Hench (1962), who injected air through perforated plates into a column of water, using a variety of orifice sizes and spacings. Results of their study are sketched in Figure 1 (using lines for clarity instead of the original data symbols, which had significant scatter in the transition zone of the upper curve). With many orifices, nearly ideal bubbly flow could be achieved, with a transition to churn flow beginning near a gas flux of 5 cm/s. With less fine orifice plates, much lower gas holdup was achieved.

Three-phase, Nonfibrous Systems

Although different flow regimes with distinct characteristics have also been observed and reported for three-phase systems (Zheng et al., 1988), many published investigations do not directly address flow regimes at all (Godbole et al., 1983; Shah et al., 1985; Sada et al., 1986; Chen and Fan, 1990). There also appears to be

considerable disagreement among investigators with respect to the definition and characterization of flow regimes in three-phase systems (Zheng et al., 1988). Nevertheless, a simple flow-regime map similar to the two-phase bubble columns, consisting of a homogeneous bubbly zone at small j_G a transition zone at intermediate j_G and a turbulent bubbly zone at high j_G appears to be adequate in many cases (Zheng et al., 1988).

Chen et al. (1994) studied gas-liquid-particle systems in a 10.2 cm vertical column with 500 μm glass and 1.5 mm acetate beads in water and in sodium iodide solution for refractive index matching. Their flow visualization study revealed that churn flow (coalesced bubble flow) can be subdivided into a vortical-spiral regime and a turbulent flow regime. The vortical-spiral flow features large vortices that begin near the surface of the fluid and descend into the column, while the central gas-rich plume (large bubbles) may rise in a helical manner coupled with lateral swinging back and forth. Flow features and flow transition conditions were similar in flows with and without particles, even for particle loadings up to 10 wt% (the highest loading for which flow visualization was possible).

Kara et al. (1982) studied a cocurrent slurry reactor with mineral residue and coal particles, using hydrostatic head measurement to determine average gas holdup. As solids concentration increased, gas holdup decreased and apparent bubble size increased. On the other hand, Sada et al. (1986) found that small amounts of fine particles can increase gas holdup in a quiescent bubble column, though in general gas holdup decreased with increasing solid loading.

A large number of correlations and models have been proposed for predicting gas and liquid volume fractions in three-phase columns (see the review by Murayama and Fan, 1985). The drift flux model, modified to account for the effect of solid particles, has also been applied (Darton and Harrison, 1975; Chen and Fan, 1990; Sada et al., 1986). The processes that strongly affect hold-up are bubble

wake hydrodynamics (Massimilla, 1959; Ostergaard, 1965; Darton and Harrison, 1975; Murayama and Fan, 1985), and particle-bubble interactions (Godbole et al., 1983). The presence of particles can in particular affect bubble coalescence and break-up. Contradictory results, however, have been reported, and it appears that particles which are wettable (i.e., have large contact angles with the liquid) augment bubble break-up, while non-wettable particles may help coalescence (Godbole et al., 1983).

Pulp Systems

Pulp fibers have a density close to the density of water and, when dispersed as isolated particles, can respond to local velocity gradients and turbulent eddies relatively fast. Most importantly, pulp fibers have the tendency to flocculate and form a network structure. Flocculation can take place in a water-pulp mixtures at consistencies as low as 0.3%, and for consistencies above roughly 1%, continuous fibrous networks form (Bennington et al., 1989). Network extent and strength increases with increasing consistency, creating local areas of high fiber concentration. Flocs can trap bubbles, preventing their rise through the suspension. Bubble streams must bypass flocs or coalesce into bubbles with enough buoyant force to break through the network. In stagnant pulp, bubbles are likely to flow through channels with lower hydraulic resistance.

Flocculation, even at low consistencies, renders the hydrodynamic characteristics of fibrous pulp mixtures quite different than those observed in other three-phase flow systems. At low shear, the network structure imparts a high apparent viscosity. Flocs may break up under shear, resulting in various macroscopic length scales in the fluid that yield complex friction loss curves for pipes. Under high shear, interaction of the fibers with fluid turbulence can lead to drag reduction (Lee and Duffy, 1976).

Serious research relevant to the hydrodynamics of gas-sparged fibrous pulp slurries has been reported only recently, and published studies are few. Walmsley (1992) performed experiments in 2-D (cylindrical) and 3-D (rectangular) transparent columns using batch fiber suspensions in the 0 - 2% consistency range. With the addition of only 0.1 wt% pulp, he noticed significant hydrodynamic changes. He could recognize bubbly and churn flow regimes. Fibers seemed to induce bubble coalescence, causing the development of churn flow at lower values of j_G in comparison with a two-phase water-air bubbling pool.

Bubble characteristics in newsprint pulp were studied by Ajersch et al. (1992), who found bubble diameters to be approximately normally-distributed. Pelton and Piette (1992) measured the probability of bubble escape through quiescent pulp suspensions in the 0.3% to 1.5% consistency range. Adhesion of bubbles to fibers was not observed. Instead, bubble entrapment in floc networks was noticed, and bubble escape occurred when bubble buoyancy overcame the network resistance.

Pan et al. (1992, 1993) have theoretically and experimentally investigated some aspects of bubble-ink particle interactions in flotation cells. Stokesian dynamics and rigorous hydrodynamics were used to show how multiple bubbles may interact with themselves and with ink particles (Pan et al., 1992). A statistical, global flotation model was also developed (Pan et al., 1993) to estimate overall flotation performance as a function of bubble capture radius and flotation dwell time. The models neglect the effect of fibers on the macroscopic and microscopic flow fields, though the addition of rod-like elements to the hydrodynamic model is planned.

Empirical studies of flotation deinking cells provide some macroscopic information. For example, it is well known the relationship between ink removal and air injection rate shows an absolute maximum, after which further increases in air flow lead to decreased ink removal. For a specific flotation design, Pfalzer (1982) found that the maximum ink removal occurred when the air-to-pulp volumetric

flow ratio was 0.3. The falling ink removal for higher air flow rates was ascribed to the effects of turbulence. Ink removal decreases rapidly with pulp consistency above some critical value, typically between 1 and 1.5 wt %.

More research is needed in order to understand the hydrodynamic characteristics of bubbling pulp slurries and to establish a sound basis for designing and operating these systems.

EXPERIMENTAL WORK

The effect of paper fibers on flow structure in vertical bubble columns has been examined. Two bubble column systems were used, one for quiescent liquid sparged with air and the other a cocurrent flow system with throughflow of both pulp and air. Both systems were run with water-air and pulp slurry-air mixtures under similar conditions to allow the effect of fibers to be identified. Time-averaged gas distribution was measured with gamma densitometry to provide data on the multiphase flow structure. The intent was to avoid the numerous complications present in actual flotation deinking cells and focus on relatively simple fiber-water-air systems without ink particles or deinking chemicals. Such an approach should provide some basic information about fiber-water-air flows and their structure that could be compared to existing knowledge for multiphase flows.

Figure 2 is a schematic of the quiescent liquid test apparatus, the main components of which are a cylindrical transparent column (the test section), an air flow system, and a gamma-ray densitometer and its electronics. The test section was a transparent cylinder with 12.7 cm inner diameter, 66 cm height, and 0.64 cm wall thickness. Air was injected at the base of the column using a perforated rubber plate with approximately 230 holes. The holes were drilled with a 2.4 mm bit, and were arranged in a square lattice with 0.7 cm pitch. The air flow rate was measured using

a Hastings Model PR-4A Four Channel Flow Meter. (Details are given in Taylor, 1993.)

Figure 3 shows the cocurrent flow system, which consists of a 1.5 m long transparent column with an internal diameter of 12.7 cm. Air and flowing slurry are mixed in a 2.5-cm pipe prior to a conical diffuser. Air flow was driven by the regulated gas pressure (as opposed to a venturi injector, in which air flow is dependent on liquid flow). Gas flow was monitored with a Hastings mass flowmeter; superficial velocities of 0 to 4.2 cm/s were used. Gas dispersion was caused by shear in the 2.5-cm injection line, where liquid Reynolds numbers were on the order of 10^4 for the conditions of this study. Pulp was continuously pumped through the system using a Diskflow™ pump monitored with a magnetic flowmeter. Superficial pulp suspension velocity ranged from 2.5 to 7.5 cm/s. A holding tank was used to separate air from the slurry before the slurry is pumped back to the test column. (Details are given in George, 1994.)

The gamma-ray densitometer, used on both pulp systems, includes a 45 mCi Am-241 source and an Ortec Model 276 detector. Principles of gamma densitometry can be found elsewhere (Honan and Lahey, 1978; Vince and Finckle, 1983). The gamma-ray densitometer was used for measuring chord-average void fractions at various locations in the test section. To make this possible, a bracket was designed and built to support the gamma source and the detector, which allowed for axial and lateral movement of the densitometer, ensuring that the collimated gamma beam and the detector remained aligned.

The heights at which gamma-ray densitometry was performed in the quiescent liquid apparatus are designated as Planes h_0, h_1, etc., as shown in Figure 2. In the quiescent liquid apparatus, adjacent planes were 5.1 cm apart, and Plane h_0 was 8.9 cm above the test section bottom. Gamma-ray densitometry was performed on 9 chords in each measurement plane. Adjacent chords were approximately 1.3 cm

apart. In the cocurrent flow apparatus, measurements were made at heights of 30.5, 50.8, 71.1, 91.4, 111.8 and 132.1 cm above the outlet of the conical diffuser. Nine equally spaced chords were also used in each plane. Table 1 lists the radial offset (distance from the chord midpoint to the centerline of the column) and length of each chord for both the quiescent liquid and cocurrent flow columns.

Quiescent Liquid		Cocurrent Flow	
Radial offset, cm	Chord length, cm	Radial offset, cm	Chord length, cm
5.40	6.69	5.60	5.99
-4.76	8.40	-4.90	8.08
4.13	9.65	4.30	9.35
-3.49	10.61	-3.60	10.46
2.86	11.34	2.90	11.30
-2.22	11.90	-2.20	11.91
1.59	12.30	1.50	12.34
-0.95	12.56	-0.80	12.60
0.32	12.68	0.20	12.69

Table 1. Radial offset and length of the chords used for gamma densitometry measurements at various planes in the quiescent liquid and cocurrent flow bubble columns.

The pulp slurry used in all pulp tests was produced from commercial unprinted newsprint composed primarily of southern softwood. The slurry was prepared by soaking the pulp in distilled water for several hours, followed by disintegration at roughly 10 wt% consistency in a laboratory repulper. The pulp was then diluted with distilled water to 1 wt% and 2 wt% slurries. The commercial newsprint contained some residual surfactant, enough to promote some foaming

when bubbled with air. The surface tension of liquid water filtered from the 1% slurry was measured at 56 dyn/cm, a 22% reduction from that of pure water.

Before each test in the quiescent fluid apparatus, the test section was filled with four liters of water-pulp mixture at the desired consistency. The gamma-ray densitometer was calibrated for each of the aforementioned 45 chord locations (nine chords, five horizontal planes) separately. This was done by measuring the gamma beam attenuation twice, once with the test section empty, the other with the test section full with the water-pulp slurry (Honan and Lahey, 1978). Calibration measurements, as well as all gamma-ray densitometry measurements to be discussed later, were each repeated three separate times and then averaged. Similar procedures were applied for the cocurrent flow system, though longer averaging times were used for most runs rather than triple replication of gamma count measurements.

Following the completion of gamma-ray densitometer calibration, the air flow was adjusted at desired levels. The system was allowed to run for several minutes to ensure steady-state, and the gamma-ray densitometry measurements were performed at all chord locations. These measurements were repeated with pure water, and with 1% and 2% consistency water-pulp mixtures (2% consistency data are not available for the cocurrent flow system due to the difficulty of removing the entrained air from the pulp prior to recirculation).

An interesting characteristic of paper pulp suspensions, which makes them distinct from other slurries, is the former's capability to trap and maintain relatively significant amounts of gas, well after the flow of the throughput gas has been terminated. To study this phenomenon, a number of tests in the quiescent liquid apparatus were also performed to determine the effect of air superficial velocity during the operation of the apparatus on the amount of air that remained in the suspension mixture after the air flow was stopped. In each of these tests the air was

initially allowed to flow at the desired rate for at least 30 seconds before the air flow was abruptly stopped. In order to allow for completion of bubble movement, gamma-ray densitometer counts were not recorded for at least 30 seconds after the air flow was stopped. Gamma-ray densitometry was then performed at all nine chord lengths at elevation h_2 (19.1 cm, see Figure 2). These chord-average void fractions were then used in calculating the cross-sectional average void fraction on plane h_2, according to

$$\varepsilon_{G,j} = \frac{\sum_{i=1}^{9} \varepsilon_{G,i,j} \ell_i}{\sum_{i=1}^{9} \ell_i} \tag{1}$$

where ε_G is the volume fraction of the gas (void fraction), and subscripts j and i are indices representing horizontal planes and chords, respectively. For the aforementioned calculations of the void fraction at Plane h_2, j=2 in Equation 1.

The uncertainty associated with the gas hold-up measurement by gamma-ray densitometry was calculated using the methodology of Honan and Lahey (1978). Accordingly, the calculated maximum relative errors, $\Delta\varepsilon_G/\varepsilon_G$, were 20% for ε_G = 0.015, 2% for ε_G = 0.11, and less than 1% for $\varepsilon_G \geq 0.22$.

The pool-average void fraction in the quiescent liquid tests could be obtained in two ways: by using the swell level height; or by volume-averaging the measured chord-average void fraction data from gamma-ray densitometry. These are explained below.

According to the first method, the pool-average void fraction was calculated from:

$$\bar{\varepsilon}_{G,SL} = 1 - H_0 / H \tag{2}$$

where H_o represents the collapsed water level height in the column, and H represents the swell level height during the tests. Measurement of H was relatively simple for the pure water and pulp solutions at low air flow rates. At high j_G, however, the exact pool surface height was difficult to specify due to the waves resulting from frequent departures of large bubbles. For pure water tests the pool level height fluctuations resulted in an estimated maximum absolute uncertainties of $\Delta\bar{\varepsilon}_{G,SL} \approx \pm 0.02$. In tests with 1% and 2% consistency, the amplitudes of swell level height oscillations were larger, resulting in estimated maximum absolute uncertainties of $\Delta\bar{\varepsilon}_{G,SL} \approx \pm 0.03$.

In the second method of calculating the pool average void fraction, the volume-average void fraction representing the portion of the column below Plane h_4 (see Figure 2) was obtained from:

$$\bar{\varepsilon}_{G,h_4} = \frac{\sum_{j=o}^{4}\sum_{i=1}^{9}\varepsilon_{G,i,j}\ell_i}{5\sum_{i=1}^{9}\ell_i} \tag{3}$$

Estimation of Radial Gas Distribution from Chord Averages

In a given horizontal plane of axisymmetric flow in a vertical bubble column of inner radius R, the relationship between the radial distribution of gas holdup, $\varepsilon(r)$, and a chord averaged holdup, E_i, at a radial offset r_i from the centerline, is

$$E_i = \frac{1}{L}\int_0^L \varepsilon(r(\ell))d\ell \tag{4}$$

where ℓ is the distance along a chord of length L, and $r(\ell)$ is the radial distance from the center of the column to point ℓ on the chord. Distances $r(\ell)$ and L are given by

$$r(\ell) = \left(r_i^2 + \left[\frac{L}{2} - \ell\right]^2\right)^{1/2} \tag{5}$$

and

$$L = 2\sqrt{R^2 - r_i^2}\,. \tag{6}$$

With a simple inverse method, a set of N discrete chord average measurements could be used to obtain local radial holdup values for N discrete annular rings in the bubble column by defining each radial offset to be the midpoint of a discrete annular zone. The discrete values ε_i then represent the average holdup in each annular ring. The relationship between ε_i and a measured chord average, E_i, is simply

$$M_{ij}\varepsilon_j = E_i \tag{7}$$

where **M** is an upper diagonal matrix in which the characteristic component M_{ij} represents the fraction of measurement chord *i* occupied by annulus *j*. Backward substitution solves for ε_j.

In using the chord-averages to estimate the annular gas distribution, several difficulties are encountered. The mapping matrix, M, has significant off-diagonal values and a small determinant (e.g., 0.01 for 5 annuli and 8×10^{-5} for 8 annuli, using equally spaced radial zones) which can inflate the effect of measurement error on the computed annular distribution. For example, in calculating the apparent holdup of the central core, one can use a chord average passing through the center and previously calculated annular holdups for outer rings to solve for the central holdup. However, the central zone represents only a fraction of the total chord used in the measurement, having only a weak influence on the chord average, but error in the measurement will be reflected only in the computed value for the central zone and will be magnified there. If raw chord data are directly inverted to obtain radial holdup values, impossible holdup values (less than zero or greater than one) for some zones may be obtained, especially when there are sawtooth-like fluctuations in the raw data. For reasonable results, a smooth curve must be used to represent the

data. A quadratic curve fit is sufficient to capture the typical distribution of chord averages. Values from the quadratic curve at the midpoints of the radial zones are then used with the mapping matrix to solve for the radial distribution.

RESULTS AND DISCUSSION

Pure Water Tests, Quiescent Liquid Apparatus

These tests were performed in order to provide reference data to facilitate the interpretation of the tests with pulp slurries. Representative measured chord-average gas volume fraction profiles are depicted in Figures 4 through 7, with ascending gas superficial velocities. The radial distributions are the distributions of chord averages as a function of radial offset from the centerline. For simplicity, Figures 4 and 5 only show data at three vertical locations, since the values at other locations are similar to those shown. Figure 4 shows four groups of data for four gas superficial velocities, ranging from 0.79 to 2.63 cm/s. In this bubbly flow regime, gas holdup is a nearly linear function of j_G, the gas distribution is relatively flat across the column, and the radial chord average distribution is fairly constant with vertical position. A transition from bubbly to churn flow seems underway for the data at j_G = 3.95 cm/s in Figure 5. In the new flow regime at higher gas flow (Figures 5 to 7), the profiles show stronger gradients in the radial and vertical directions.

The apparent asymmetry in the radial profiles is due to asymmetry in the radial offsets for the chords on the right and left sides of the column. The rightmost chord (positive radial offset) occurs at r = 5.6 cm, while the leftmost chord is at r = -4.9 cm. Even if the flow is perfectly axisymmetric, data at r=5.6 cm are much closer to the wall (r=6.35 cm) and will have a lower holdup (for typical gas distribution patterns) than data at r=-4.9 cm. The asymmetric placement of the chords should be kept in mind in examining all profiles across the column.

The observed flow phenomena in water were generally consistent with those reported by other investigators (Chen et al., 1994; Shah et al., 1982; Shenderov and Dilman, 1989). Based on visual observations, for $j_G \leq 3$ cm/s the flow regime in the column was distinctly bubbly, and the system was characterized by a homogeneous mixture of bubbles rising along rectilinear paths. The flow regime in the 3 cm $\leq j_G \leq 6$ cm/s range represented transition from bubbly to churn-turbulent flow. With $j_G \geq 6$ cm/s the flow regime was distinctly churn-turbulent, characterized by the arrival of very large bubbles at the swell level. The churn-turbulent data, represented by Figures 6 and 7, show a monotonic increase in ε_G as the centerline is approached, indicating a nonuniform lateral distribution. This lateral nonuniformity was evidently due to the formation of large, fast-moving bubbles near the center, which are formed due to strong bubble coalescence. Recirculatory flow down the column walls was also evident in the transition and churn-turbulent regimes.

Figure 8, another view of the data in Figure 6, shows holdup as a function of height along chords having four different radial offsets. The cross-sectional average holdup at each horizontal plane, calculated according to Equation 1, is also shown. Average holdup increases steadily with height in this set of data. The increase may be partially due to the additional entrainment of gas that occurs via sloshing and churning of the liquid near the top of the column in the churn-turbulent regime.

The column-averaged gas volume fractions, $\bar{\varepsilon}_{G,SL}$ and $\bar{\varepsilon}_{G,h_4}$ calculated with Equations 2 and 3, respectively, are depicted in Figure 9, where they are also compared with predictions of several widely-used empirical correlations. For $j_G \leq 1$ cm/s, where the flow regime is low-void fraction bubbly, there is good agreement between our data and the correlations. Poor agreement between the data and all the correlations can also be noted for 3 cm/s $\leq j_G \leq 6$ cm/s, representing the region of bubbly to churn-turbulent transition. In the churn-turbulent regime the data reason-

ably agree with the correlation of Kumar et al. (1976). Significant disagreement among various correlations, in particular at high j_G, is also noted.

The following are possible reasons for the relatively poor agreement between our data and the correlations depicted in Figure 9:

1. Bubble columns operating with air and water are divided into two broad categories (Shah et al., 1982). In large ($D_C \geq$ roughly 15 cm) columns, the churn flow regime is obtained at high gas superficial velocities, where gas hold-up is only weekly affected by the column size. In small columns (D<15 cm), on the other hand, slug flow dominated by large Taylor bubbles may occur at high gas superficial velocities. The above correlations are mostly based on data obtained with large columns. However, Taylor bubbles were not observed in the 13-cm columns of this study. In contrast to the 15-cm criteria of Shah, a study of Ellis and Jones (1965) in gas-liquid bubble columns indicates that gas holdup is not a function of column diameter for columns greater than 7.5 cm in diameter. Gas holdup is increased by wall effects for more narrow columns.
2. All of the above correlations are based on data including relatively high superficial velocities. An exception is the correlation due to Kumar et al. (1976), for which the data base covers $j_G \leq 14$ cm/s.
3. The experimental data show relatively wide scatter, and are sensitive to the method of gas injection. Our data, for example, fall within the experimental data compiled and depicted by Bach and Pilhofer (1978).
4. The drilled rubber disk gas injector may give an unusually fine and uniform gas distribution that allows better holdup than other injector systems. In the early stages of this study (Lindsay et al., 1994), experimental work with other gas distributors such as sintered metal diffusers gave significantly lower gas holdup in water, much closer to the correlations in Figure 9.

Pulp Slurry Tests, Quiescent Liquid Apparatus

1% Consistency Pulp Results. Figures 10 and 11 depict representative profiles of chord-average void fractions for tests with a 1 wt% fiber slurry. Figure 10 shows three sets of data for $j_G \leq 2.63$ cm/s, with only three planes of data per set shown for simplicity. Figure 11 shows typical results for higher superficial gas velocities, reported only at the 19.1 cm plane; for each gas velocity, there was a significant vertical gradient, similar to those shown in Figure 10. Compared to the results for similar flow conditions in pure water, the pulp slurry shows lower holdup values. The profile sets show greater variation with height (a monotonic increase in ε_G with height), and stronger radial gradients. Such features resemble those observed in water in the transition regime between bubbly flow and churn-turbulent flow (see Figure 5). The presence of fibers appears to promote a flow regime characterized by bubble coalescence even for low j_G values that would give bubbly flow in water.

The decreased gas holdup relative to pure water can be explained by increased bubble coalescence caused by a fibrous network. Small bubbles, which normally have long dwell times, are impeded by the fiber network (Pelton and Piette, 1992). A bubble held in place by a flow or network structure is soon joined by other rising bubbles, until coalescence yields a bubble with enough buoyant force to break through the restriction. At this point, the bubble begins to rise rapidly and can have a much smaller dwell time than the original small bubbles would have had in pure water. The result is a net decrease in gas holdup (though Walmsley, 1992, also noted that fibers will increase gas holdup if the consistency is so dilute that flocs do not form; such a consistency may be on the order of 0.1 wt%). Further, if the pulp consistency is high enough or if the gas flow rate is high enough, the gas may rise in distinct channels, resulting in very low residence time and low average holdup. Slight agitation could destroy the channels.

Because of the opacity of the pulp slurry, visual observation of flow patterns and bubble hydrodynamic phenomena were limited to the regions adjacent to the column wall, and near the mixture swell level. Observations indicated that the flow regime for $j_G \leq 1.32$ cm/s was bubbly. While visual cues suggested a bubbly flow regime at low j_G, the fibrous slurry undoubtedly promoted coalescence, as evidenced by the lower gas holdup. At higher superficial gas velocities, the flow in 1 wt% pulp displayed obvious churning features and large vortices, consistent with the flow mechanisms discussed by Chen et al. (1994), though flow structure inside the column was not visualized.

The increase in gas holdup with column height in an apparently (based on visual appearance) bubbly flow of 1% pulp ($j_G \leq 1.32$ cm/s) was not expected. In spite of the lack of strong churning at the top of the column, recirculatory flow may partially account for the observed positive vertical gradient in ε_G. At the top of the column, fine air bubbles were formed in a froth, apparently due to natural or residual industrial surfactants in the pulp (some bubble dispersion by weak churning may have been present as well). These small bubbles can be carried back down into the flow by the descending fluid along the column walls. Recirculation ceases as the bottom of the column is approached, and the gas content of the descending fluid may decrease with decreasing height as fine bubbles coalesce and rise. These mechanisms could then impart an overall vertical gradient in gas holdup, with higher gas holdup near the surface of the slurry pool. It is possible that opposite trends or more uniform vertical distributions may be encountered, depending on the relative importance of churning, recirculation, and coalescence in the system.

In the tests at $j_G = 0.79$ cm/s, because of the absence of strong recirculation in the lower section of the column, the fiber tended to build up at the column base and near the column wall. The resulting pulp formations were responsible for the small

values of chord-averaged ε_G values for the chords nearest the wall in Figure 10. Minor pulp buildup near the base was also observed in the test with j_G = 1.32 cm/s. Pulp buildup was not apparent in the other tests, evidently due to stronger recirculatory flow.

Figure 12 shows holdup in 1% pulp with j_G = 6.58 cm/s as a function of height along chords having four different radial offsets; this figure is comparable to Figure 8 for water. The flow in this case showed strong churning. As with pure water, average holdup increases with height. The increase may be due to the additional entrainment of gas that occurs via sloshing and churning of the liquid near the top of the column in the churn-turbulent regime. The cross-section averaged holdup is significantly less in the 1% pulp than in water.

2% Consistency Pulp Results. Representative chord-average gas holdup profiles are shown in Figure 13 at the 19.1 cm horizontal plane and in Figure 14 for j_G = 2.63 cm/s at three horizontal planes. The holdup profiles show pronounced asymmetry and stronger radial gradients than seen in typical profiles from the 1% pulp, indicating different hydrodynamics. Once again, due to the opacity of the slurry, effective visual observations were limited to the vicinity of the swell level and the transparent column walls. These observations, along with the recorded void fraction profiles, indicated that the flow field in the column was dominated by the formation of three-dimensional pulp networks which resulted in channeling phenomena. Channeling could be seen along the column walls, as trains of large coalesced bubbles built up and rose along relatively well-defined and persistent paths. Bubble coalescence, which evidently occurred even at very low values of j_G, can be attributed to the fiber flocculation and the consequent channeling that also reduced the effective gas flow area. This reduction in flow area results in higher gas velocities in the channels, leading to stronger bubble coalescence and the formation of large bubbles. Also, at low j_G, due to the absence of strong recirculation, the fibers

tended to settle, causing an increase in the fiber consistency near the bottom of the test section.

Three dimensional flock networks, resulting in tortuous channels, are consistent with the large variations seen in chord averages at various heights for $j_G \leq$ 2 cm/s, such as those shown in Figure 15 for j_G = 1.97 cm/s. As j_G is increased, abrupt axial variations of chord-average void fractions become fewer, as evidenced in Figure 16, perhaps because stronger gas flow reduces the tortuosity of channels (becoming more vertical rather than meandering) and possibly because more intense fluid motion (churning) regularly breaks down channel paths, causing new temporary channel paths to form. Channeling still occurs, nevertheless, and lateral nonuniformity in ε_G persists. (Details of the channel structure and internal hydrodynamics are only inferred from visual observation of external surfaces and are thus subject to uncertainty in interpretation.) The channels appeared to form preferentially approximately half way between the column wall and its center.

There was little of the foaming action on the surface of the 2% pulp pool that was seen on the surface of the 1% pulp pool surface.

Pool-Average and Residual Void Fractions

Figures 17 and 18 show plots of $\bar{\varepsilon}_{G,h_4}$ and $\bar{\varepsilon}_{G,SL}$, calculated with Equations 3 and 2, respectively, versus superficial air velocity. Some of the differences between the two methods may be due to the difficulty of establishing pool height under strongly churning conditions. In general, both methods show the significant decrease in holdup caused by the presence of the fibers. The $\bar{\varepsilon}_G$ profiles for 1% and 2% consistencies both indicate that, for $j_G \geq$ 5 cm/s, further increases in j_G result only in a slight increase in $\bar{\varepsilon}_G$. The trends resemble those shown in Figure 1, where coarser orifices reduced gas holdup in pure liquid and promoted transition to a coalesced bubble flow regime.

Many empirical correlations have been suggested for predicting the pool-averaged gas or liquid volume fractions in three-phase columns. Most of the correlations, however, only apply to fluidized beds and therefore deal with large solid particles significantly denser than the liquid phase (Murayama and Fan, 1985). These correlations are thus inapplicable to our data.

The cross-sectional average residual void fractions representing Plane h_2 (19.1 cm elevation) are depicted in Figure 19. These holdup values, as mentioned before, were measured with gamma densitometry after the air flow was shut off, and represent entrapment of small air bubbles in the fibrous networks. The bubble entrapment monotonically increases with increasing consistency and increasing the initial gas superficial velocity. The ability of the network to retain air affects the bubble size required to break through the network and affects the amount of air that the downward recirculation flow can bring back to the column, which in turn will affect the gas distribution.

There was also a noticeable change in the distribution of the pulp fibers after the air flow was turned off. For the 1% pulp, the fibers would clump into regions of greater consistency (flocs). These regions appeared roughly spherical and had an average diameter of approximately 1 cm. For the 2% pulp, channels of lower consistency were visible after the termination of all air flow rates. The channels became better defined and greater in number as the initial air flow rate increased.

The transformation of chord-averaged results to estimates of the axisymmetric radial gas distribution be presented below, following presentation of the cocurrent column results.

Cocurrent Flow Results

Figures 20-23 show chord-averaged gas-holdup profiles in the cocurrent flow column for water and 1% pulp at two different flow conditions: j_L = 2.5 or 5 cm/s, and j_G = 2.1 cm/s. The two liquid superficial velocities for water have little impact

on the gas holdup, except to provide a more uniform gas distribution at the lowest horizontal plane, 30.5 cm. At the lower liquid flux in Figure 20, the gas distribution at the lowest measurement plane appears bimodal. Observation showed that the gas plume ascending from the conical expansion tended to stay close to the wall of the expansion section, possibly a Coanda effect. Strong recirculation zones would exist in the regions of the expansion port not containing the plume. The plume would oscillate from side to side with an apparently unsteady frequency on the order of 1 Hz or higher. Since gamma densitometry measurement times in this system were on the order of 30 seconds per chord, the oscillating plume leads to a bimodal gas distribution measured at the lowest plane. Following the expansion zone, the plume would ascend into slower moving liquid and disperse due to large scale mixing, resulting in more symmetric gas distribution patterns.

Figures 22 and 23 show similar features to the water results, with two differences: (1) results in the lowest horizontal plane at the lower gas flux (Figure 22) are asymmetric but monomodal in gas distribution, suggesting that the plume was stabilized (nonoscillating) in pulp flow; and (2) the gas holdup values in pulp flow are higher than in water flow at similar gas and liquid fluxes. Unlike flow in the static column, the gas holdup in a 1% consistency pulp in the cocurrent flow system was generally found to be higher than the gas holdup in pure water at various combinations of liquid and gas flow rates. The reasons for this behavior are discussed later in this section. The radial distribution of the chord-averaged gas holdup appears parabolic, commonly having a centerline average holdup two or three times the values at the wall. The conversion of chord averages to radial distribution values is treated in the following section.

As a rule, flow regimes in the cocurrent flow column resembled those in the quiescent column, with bubbly flow in water at low gas velocities (j_G roughly < 4 cm/s), followed by flow with a churn-turbulent nature at higher gas velocities. In

pulp, the flow had a churn-turbulent nature at lower velocities, though only the outer portion of the flow could be seen. What appeared to be churn-turbulent flow in some cases may have been a transition regime from bubble to churn-turbulent flow, for the gas holdup curves (holdup versus gas velocity) for pulp and for water were linear over the limited range of gas flow rates used. However, in pulp flows at the higher gas flow rates, some large bubbles were visible, with diameters on the order of 2-5 cm, which created large, swirling eddies in the flow as they rose, indicative of churn-turbulent flow and similar to the spiral-vortical flow described by Chen et al. (1994). Precise identification of flow regimes in the future will require examination of transient differential pressure measurements across the column to obtain information not available by visual inspection.

The cocurrent flow results also tended to have flatter profiles of chord averaged holdup versus radial offset than was seen in the quiescent system, and showed less variation in holdup profiles with height. The bulk flow of the liquid may have weakened the central plume and the associated recirculatory flow, leading to a flatter velocity and gas distribution. However, visual observation did show the presence of recirculatory flow across most of the column under typical flow conditions.

To see that gas holdup increases with the addition of fibers, consider $\bar{\varepsilon}_G$ (column-averaged gas holdup, averaged over cross sectional area and over column height) as a function of j_G, as plotted in Figures 24-26. Part of the increased gas content in the pulp flow may be due to entrainment of air in the pulp as it flows from the holding tank back to the pump. For example, extrapolation in Figure 24 of the pulp curve to an injected gas flux of zero gives a holdup of 2%, indicating that 2% air content was present in the pulp as it left the holding tank. If so, the difference between the pulp and water results in Figure 24 may be due primarily to extra air that was present in the pulp before passing through the air injector. However, at

higher liquid flow rates (Figures 25 and 26), the higher holdup in the pulp relative to water cannot be explained by higher initial air loading alone (in fact, the extrapolated air content at zero injected gas flux is about 2% for both water and pulp suspensions at the two higher pulp flow rates). In Figures 25 and 26, the liquid superficial velocity is greater than the gas superficial velocity for all measurements (higher air flow rates increased pressure drop and increased air accumulation in the pump, hindering pump operation). Under these conditions, the dispersed bubbles, slowed in their ascent by the fibers, can be carried away by the pulp flow before other bubbles rise and coalesce with them. It seems that fibers cause coalescence when small bubbles cannot break through the network rapidly enough to avoid being hit by subsequent bubbles, and that aggregation continues until a large bubble has enough buoyant force to escape. When the pulp itself is flowing upwards as well, bubbles can avoid collisions by being carried away before later bubbles arrive.

Estimates of Axisymmetric Radial Gas Distribution

Chord-averaged radial profiles of gas holdup can be used to estimate the axisymmetric radial distribution of holdup using the inverse procedure described in the Experimental section above. For example, consider data from the cocurrent flow facility with 1% pulp, taken at a height of 30.5 cm with j_L = 5 cm/s and j_G = 0.56 cm/s. Figure 27 shows the raw data, a quadratic fit to the data, and the computed axisymmetric radial gas distribution for choices of 5 and 8 annular zones, both with uniform radial spacing. Little difference is seen between the two zone spacings, suggesting the method is relatively insensitive to the number of rings chosen. The data and the quadratic curve fit are not completely symmetric about the centerline, whereas use of Equation 7 to obtain ε_i assumes radial symmetry. The curve fit is averaged about the centerline, which in effect reduces an expression of the form $E_i = a + br + cr^2$ (for $-R<r<R$) to $E_i = a + cr^2$ (for $0<r<R$). (In cases of purely axisymmetric data, the first-order coefficient b will be zero.)

The computed axisymmetric radial gas distribution in Figure 27 shows a central gas holdup value roughly 30% greater than the chord averaged holdup for the chord that passes through the central zone. The difference between the computed holdup at the centerline and the measured holdup for a central chord depends on the flatness of the measured chord-averaged distribution. If the holdup varies strongly with radial offset, the computed radial holdup distribution will vary even more strongly with radial position. An example is given in Figure 28, which compares chord-averaged data and computed radial gas distributions in the quiescent flow system for both water and pulp with j_G = 2.63 cm/s at an elevation of 19.1 cm. The chord averaged holdups in water show less variation with radial offset than do the results in 1% pulp. As a result, the computed radial gas distribution diverges more strongly from the chord-averaged distribution in the case of pulp than in water. With pulp, the computed central gas holdup is 40% greater than is indicated by the chord averaged distribution.

Chord-averaged results can be reduced to radial gas distribution values for all planes of measurement under a single flow condition to yield a 3-D portrayal of the computed axisymmetric gas distribution, as shown in Figure 29 for the cocurrent flow system with 1% pulp, j_L = 2.5 cm/s, and j_G = 3.1 cm/s. The high gas flow in this case produces a strong radial gradient in gas holdup, with centerline values nearly 5 times greater than gas holdup near the wall.

APPLICATIONS TO FLOTATION DEINKING

Though the present study represents an effort to understand basic phenomena at a level remote from the full complexities of true flotation deinking systems, several insights have been obtained with the following potential implications for flotation deinking:

1. Comparison of air flow through pulp suspensions and pure water show that fibers and flocs can induce significant changes in the spatial distribution of air, in bubble size distribution, and in the nature of the flow regime (e.g., bubbly, churn, churn-turbulent, channel flow). Unfortunately, much of the design of modern flotation deinking systems has been based on visualization studies in pure water, with the potential of inapplicable results. Undoubtedly, much room exists for improved flotation hydrodynamics.

2. Operators and vendors of flotation deinking cells have long known that flotation efficiency drops as pulp consistency exceeds a critical point (usually slightly above 1%). Vendors have also learned that efficiency will decrease when the air flow rate is increased above a certain level. The fundamental causes for these drops in efficiency have not been clearly stated or even understood in the past. The present work points to the importance of flow regimes in the behavior of flotation deinking. When consistency or gas flow rate are elevated, flow regimes with low interfacial area may be established (e.g., large bubbles or channel flow) or possibly with churning strong enough to strip attached ink particles from bubbles. Ink removal may then be reduced.

3. Cocurrent flow offers the potential for increased interfacial area and higher gas holdup by reducing floc-induced coalescence. This may be an important feature in some existing designs and may be further exploited as a design principle in the future.

4. A buoyancy-driven flow such as occurs in flotation deinking may have strong recirculation, with fluid from the surface returning toward the bottom of the cell. This recirculation may be undesirable, for it can entrain ink-laden foam back into the suspension and can also backmix the deinked pulp into the dirty pulp. Recirculation will be tied to the geometry in a flotation unit. More confined geometries should inhibit recirculatory flows. Wall effects (viscous shear) impede

recirculation, for high shear would be required to have upward flow at the center and downward flow at the walls. Instead, wall effects may promote a more uniform flow and could increase the gas holdup and the interfacial area, though a transition to Taylor bubbles (slug flow) may occur if walls are too restricting. Modifications of flow geometry perhaps should be explored to enhance flotation efficiency.

5. The mechanisms that lead to large bubbles, especially that of floc-induced coalescence, suggests that the initial bubble size distribution entering a flow system does not persist. The actual bubble size distribution in a flotation deinking cell may be only slightly linked to the original bubble size distribution. There is a need to develop techniques for determining the dynamic bubble size distribution in pulp slurries.

CONCLUSIONS

In the quiescent liquid apparatus, macroscopic flow patterns in three-phase pulp slurries with 1% and 2% consistency were experimentally studied, and were found to be significantly different than flow patterns observed in pure water or non-fibrous three-phase columns. Fiber flocculation and networking dominated the flow field. The fiber network promoted bubble coalescence and gas channeling, leading to shorter gas residence times and lower gas holdup values than in pure water. With 2% pulp consistency, the fiber network induced tortuous, three-dimensional bubble paths that became less tortuous and more frequently disrupted as gas flow increased.

Similar tests in a cocurrent flow system with water and 1% pulp confirmed a number of the results obtained in quiescent liquid flow, while highlighting a mechanism for enhanced gas holdup when the liquid superficial velocity exceeds the gas superficial velocity. In that case, even though the fibrous network impeded

the relative rise of bubbles, the bulk liquid flow may carry away bubbles before they are joined by subsequent bubbles. The bulk flow of the slurry reduces coalescence into large bubbles that could break through the network and rise rapidly, while the network simultaneously impedes the relative rise of small bubbles. As a result, overall holdup and interfacial area can be elevated.

A simple method was demonstrated to convert chord-averaged holdup values at various radial offsets into estimates of radial gas holdup distributions, assuming axisymmetric flow conditions. The computed radial gas distributions indicate centerline holdup values may be up to about 40% higher than the chord-averaged holdup for the centermost chord.

The present experimental study shows that the hydrodynamics, and therefore transport processes, in three-phase pulp slurries may not be modeled by using the models and correlations based on non-fibrous data. Systematic experimental studies addressing three-phase fibrous systems are thus needed.

ACKNOWLEDGMENT

Thanks to Tom Merchant for assistance in experimental work, to Shawn Ye for assisting in construction of necessary apparatus, and to Michael Schaepe for expert assistance in the use of radioactive materials. Thanks to Mike Walmsley, Robert Pelton, and Chi Yu for useful suggestions and discussions. Portions of this work were conducted by Jonathan George in partial fulfillment of the requirements for the M.S. degree at IPST and by Kevin Taylor in partial fulfillment of the requirements for the M.S. degree at Georgia Tech. This work was funded by a research award from the TAPPI Research Foundation and by the member companies of IPST.

NOMENCLATURE

D_C = column diameter, m

E_i = chord averaged gas holdup for chord i

g = gravitational acceleration, m/s^2

h = elevation of measurement plane, cm

H_o = collapsed slurry level height (zero void fraction), m

H = bubbling slurry level height, m

I = index for chords in gamma-ray densitometry

j = index for horizontal planes in the section

j_G = superficial gas velocity, cm/s

j_L = superficial liquid or slurry velocity, cm/s

ℓ = distance along a chord, m

L = chord length, m

M_{ij} = mapping matrix in Eq. 7

r = radial distance, r

r_i = radial offset (distance from centerline) for chord i, m

R = column radius

Greek Letters

ε = gas holdup (volumetric void fraction)

$\Delta\bar{\varepsilon}_G$ = column-averaged gas holdup

$\Delta\bar{\varepsilon}_{G,h_4}$ = column -average gas holdup from Eq. 3

$\Delta\bar{\varepsilon}_{G,SL}$ = column -average gas holdup from Eq. 2

ε_s = pulp consistency (% wt of fiber in water-pulp mixture)

Subscripts

G = gas phase

L = liquid phase

REFERENCES

Ajersch, M.; Pelton, R.; Towers, M.; Loewen, S. The Characterization of Dispersed Air in Two Newsprint Paper Machines. *J. Pulp Paper Sci.* **1992**, 18, 121.

Akita, K.; Yoshida, F. Gas Holdup and Volumetric Mass Transfer Coefficients in Bubble Columns. *Ind. Eng. Chem. Proc. Des. Dev.* **1973**, 12, 76.

Bach, H.F.; Pilhofer, T. Variations of Gas Hold-Up in Bubble Columns with Physics Properties of Liquids and Operating Parameters of Columns. *Ger. Chem. Eng.* **1978**, 1, 270.

Bennington, C.P.J.; Kerekes, R.J.; Grace, J.R. Mixing in Pulp Bleaching. *J. Pulp and Paper Sci.* **1989**, 15, 186.

Bird, R.B.; Stewart, W.E.; Lightfoot, E.N. *Transport Phenomena*; Wiley: New York, 1960.

Chen, Y-M.; Fan, L-S. Drift Flux in Gas-Liquid-Solid Fluidized Systems from the Dynamics of Bed Collapse. *Chem. Eng. Sci.* **1990**, 45, 935.

Chen, R.C.; Reese, J.; Fan, L.-S. Flow Structure in a Three-Dimensional Bubble Column and Three-Phase Fluidized Bed. *AIChE. J.*, **1994**, 40, 1093.

Darton, R.C.; Harrison, D. Gas and Liquid Hold-Up in the Three-Phase Fluidization. *Chem. Eng. Sci.* **1975**, 30, 581.

Duffy, G.G., and Titchener, A. L. Design Procedures for Obtaining Pipe Friction Loss for Chemical Pulps. *Tappi J.* **1974**, 57, 162.

Duffy, G. G.; Titchener, A.L.; Lee, P.F.W.; Moller, K. The Mechanism of Flow of Pulp Suspensions in Pipes. *Appita* **1976**, 29, 363.

Ellis, J.E., and Jones, E.L. Two Phase Flow Symposium, Exeter, England, June 1965, as cited by Mashelkar, R. A. Bubble Columns. *British Chem. Eng.* **1970**, 15, 1297.

Floccia, L. Vergleich industrieller Flotationszellen. *Wochenblatt für Papierfabrikation* **1994**, 122, 682.

George, J. Characterization of Low-Consistency Three Phase Flow Behavior. M.Sc. Thesis. Institute of Paper Science and Technology, Atlanta, Georgia, 1994.

Gilkey, M. W.; Yoshida, H. A New High Efficiency Flotation Device. 78th Annual Meeting, Canadian Pulp and Paper Association, Montreal, Canada, 1992, p. B153-B158.

Godbole, S.P.; Honath, M.F.; Shah, Y.T. Holdup Structure in Highly Viscous Newtonian and Non-Newtonian Liquids in Bubble Columns. *Chem. Eng. Comm.* **1982**, 16, 119.

Godbole, S.P.; Schumpe, A.; Shah, Y.T. Hydrodynamics and Mass Transfer in Bubble Columns: Effect of Solids. *Chem. Eng. Comm.* **1983**, 24, 235.

Govier, G.W.; Aziz, K. *The Flow of Complex Mixtures in Pipes*; Robert E. Kreiger Publishing Co.: Malabar, Florida, 1972.

Hikita, H.; Kikukawa, H. Liquid Phase Mixing in Bubble Columns. Effect of Liquid Properties. *Chem. Eng. J.* **1974**, 8, 191.

Hikita, H.; Asai, S.; Tanigawa, K.; Segawa, K.; Kita, M. Gas Hold-Up in Bubble Columns. *Chem. Eng. J.* **1980**, 20, 59.

Honan, T.J.; Lahey, R.T. The Measurement of Phase Separation in Wyes and Tees. U.S. Nuclear Regulatory Commission Rep. NUREG/CR-0557, 1978.

Hughmark, G.A. Holdup and Mass Transfer in Bubble Columns, *Ind. Eng. Chem. Proc. Des. Dev.* **1967**, 6, 218.

Kara, S.; Kelkar, B.G.; Shah, Y.T. Hydrodynamics and Axial Mixing in a Three-phase Bubble Column. *Ind. Eng. Chem. Proc. Des. Dev.* **1982**, 21, 584.

Kumar, A.; Degaleesan, T.E.; Laddha, G.S.; Hoelsher, H.E. Bubble Swarm Characteristics in Bubble Columns. *Can. J. Chem. Eng.* **1976**, 54, 503.

Lee, P. F. W., and Duffy, G. G. Relationships Between Velocity Profiles and Drag Reduction in Turbulence Fiber Suspension Flow. *AIChE J.* **1976**, 22, 750.

Lindsay, J. D.; George, J.; Merchant, T.; Baker, W. Exploring the Multiphase Flow Behavior of Flotation Processes. IPST Technical Paper Series, Number 520, Institute of Paper Science and Technology, Atlanta, GA.

Murayama, K.; Fan, L.S. Fundamentals of Gas-Liquid-Solid Fluidization. *AIChE. J.*, **1985**, 13, 1.

Ostergaard, K. On Bed Porosity in Gas-Liquid Fluidization. *Chem. Eng. Sci.* **1965**, 20, 165.

Pan, R.; Bousfield, D.; Thompson, E. V. Modeling Particle-Bubble Dynamics and Adhesion in Air Bubble/Solid Particle/Liquid Systems. *Proc. Tappi Pulping Conference*, Tappi Press, Atlanta, GA, 1992 , p. 941.

Pan, R.; Paulsen F. G.; Johnson, D.A.; Thompson, E.V. A Global Model for Predicting Flotation Efficiencies: Model Results and Experimental Studies. *Proc. Tappi Pulping Conference*, Tappi Press, Atlanta, GA, 1993, p. 1155.

Pelton, R.; Piette, R. Air Bubble Hold-Up in Quiescent Wood Pulp Suspensions. Can. *J. Chem. Eng.* **1992**, 70, 660.

Pfalzer, L. H. The Injector Cell - a Low-energy Flotation Machine. *Tappi J.* **1982**, 65(10), 73.

Sada, E.; Kumazawa, H.; Lee, C.; Iguchi, T. Gas Holdup and Mass-Transfer Characteristics in a Three-Phase Bubble Column. *Ind. Eng. Chem. Proc. Des. Dev.* **1986**, 25, 472.

Shah, Y.T.; Kelkar, B.G.; Godbole, S.P. Design Parameters Estimation for Bubble Column Reactors. *AIChE J.* **1982**, 28, 353.

Shah, Y.T.; Joseph, S.; Smith, D.N.; Ruether, J.A. Two-Bubble Class Model for Churn-Turbulent Bubble-Column Reactor. *Ind. Eng. Chem. Proc. Des. Dev.* **1985**, 24, 1096.

Shenderov, L.Z.; Dilman, V.E. Gas Motion in Bubble Reactors. *Theo. Found. Chem. Eng.* **1989**, 22, 359.

Sriram, K.; Mann, R. Dynamic Gas Disengagement: A New Technique for Assessing the Behavior of Bubble Columns. *Chem. Eng. Sci.* **1977**, 32, 571.

Taylor, K. An Experimental Investigation of a Bubbling Three-Phase Pool. MS Thesis, G. W. Woodruff School of Mechanical Engineering, Georgia Institute of Technology, 1993.

Vermeer, D.J.; Krishna, R. Hydrodynamics and Mass Transfer in Bubble Columns Operating in the Churn-Turbulent Regime. *Ind. Eng. Chem. Des. Dev.* **1981**, 20, 475.

Ulbrecht, J.J.; Kawase, Y.; Auyeung, K.F. More on Mixing of Viscous Liquids in Bubble Columns. *Chem. Eng. Comm.* **1985**, 35, 175.

Vince, A.M., and Finckle, J. R. The Relationship Between Density and Void Fraction Measurement Uncertainty in Radiation Densitometry. *Int. J. Multiphase Flow*, **1983**, 9, 449.

Wallis, G. B. One-Dimensional Two-Phase Flow; McGraw-Hill, New York, 1969.

Walmsley, M.R.W. Air Bubble Motion in Wood Pulp Fiber Suspension. *APPITA*. **1992**, 45, 509.

Walter, J.F.; Blanch, H.W. Liquid Circulation Patterns and Their Effect on Gas Hold-up and Axial Mixing in Bubble Columns. *Chem. Eng. Comm.* **1983**, 19, 243.

Zheng, C.; Yao, B.; Feng, Y. Flow Regime Identification and Gas Hold-Up of Three-Phase Fluidized Systems. *Chem. Eng. Sci.* **1988**, 43, 2195.

FIGURE CAPTIONS

Figure 1. Effect of initial conditions on gas holdup for perforated plate injection of air bubbles into a water column (Zuber and Hench, 1962).

Figure 2. Quiescent fluid bubble column.

Figure 3. Cocurrent flow test facility.

Figure 4. Chord-averaged gas holdup profiles in pure water for $j_G \leq 2.63$ cm/s, quiescent liquid apparatus.

Figure 5. Chord-averaged gas holdup profiles in pure water for $j_G = 3.95$ and 5.26 cm/s, quiescent liquid apparatus.

Figure 6. Chord-averaged gas holdup profiles in pure water for $j_G = 6.58$ cm/s, quiescent liquid apparatus.

Figure 7. Chord-averaged gas holdup profiles in pure water for $j_G = 9.21$ cm/s, quiescent liquid apparatus.

Figure 8. Gas holdup in water as a function of height for $j_G = 6.58$ cm/s at several chord positions, shown with cross-sectional averaged holdup.

Figure 9. Comparison of literature correlations to experimental data for column averaged gas holdup in pure water. Reported data includes gamma densitometry and pool height methods.

Figure 10. Chord-averaged gas holdup profiles in 1% pulp slurry for $j_G \leq 2.63$ cm/s, quiescent liquid apparatus.

Figure 11 Chord-averaged gas holdup profiles in 1% pulp slurry at h = 19.1 cm for $j_G \geq 3.95$ cm/s, quiescent liquid apparatus.

Figure 12. Gas holdup in 1% pulp as a function of height for j_G = 6.58 cm/s at several chord positions, shown with cross-sectional averaged holdup.

Figure 13. Chord-averaged gas holdup profiles in 2% pulp slurry at h = 19.1 cm, quiescent liquid apparatus.

Figure 14. Selected chord-averaged gas holdup profiles in 2% pulp slurry for j_G = 2.63 cm/s, quiescent liquid apparatus.

Figure 15. Gas holdup in 2% pulp as a function of height for j_G =1.97 cm/s at several chord positions, shown with cross-sectional averaged holdup.

Figure 16. Gas holdup in 2% pulp as a function of height for j_G = 6.58 cm/s at several chord positions, shown with cross-sectional averaged holdup.

Figure 17. Column-averaged gas holdup values based on gamma densitometry for water and pulp as a function of superficial gas velocity.

Figure 18. Column-averaged gas holdup values based on pool height change for water and pulp as a function of superficial gas velocity.

Figure 19. Residual gas holdup values averaged over the cross section of Plane h2 (19.1 cm elevation) for 1% and 2% pulp.

Figure 20. Chord-averaged gas holdup profiles for water in the cocurrent flow column with a liquid flux of 2.5 cm/s and a gas flux of 2.1 cm/s.

Figure 21. Chord-averaged gas holdup profiles for water in the cocurrent flow column with a liquid flux of 5 cm/s and a gas flux of 2.1 cm/s.

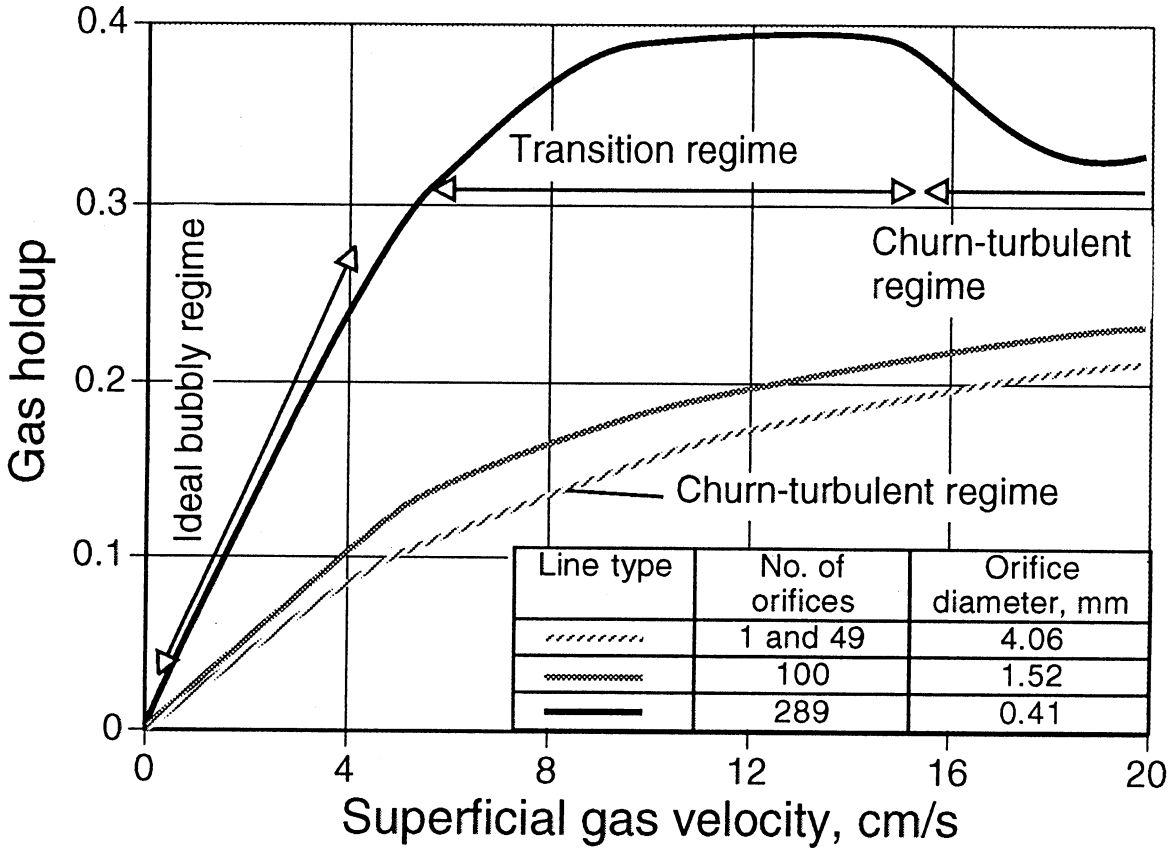

Figure 1. Effect of initial conditions on gas holdup for perforated plate injection of air bubbles into a water column (Zuber and Hench, 1962).

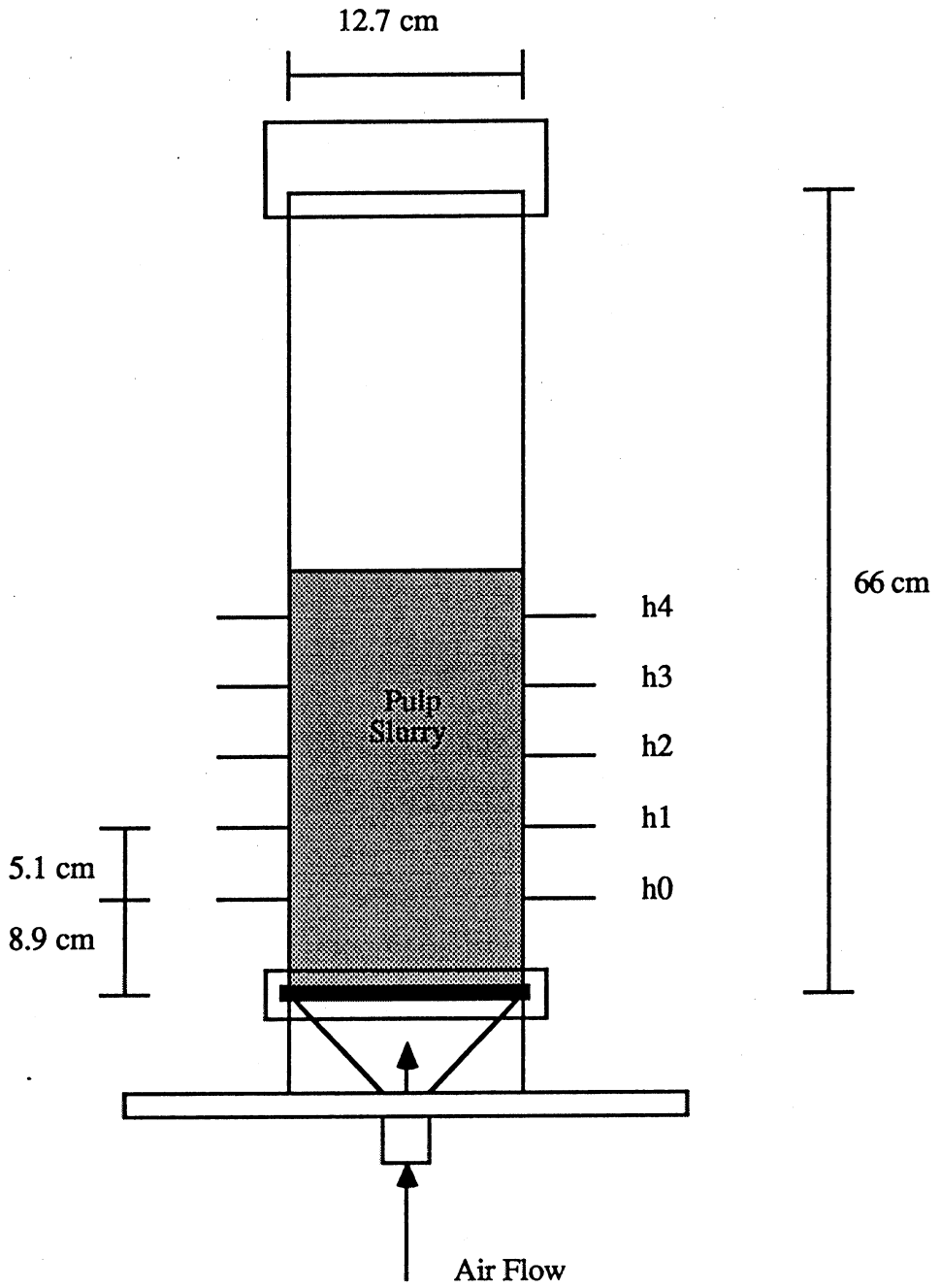

Figure 2. Quiescent fluid bubble column.

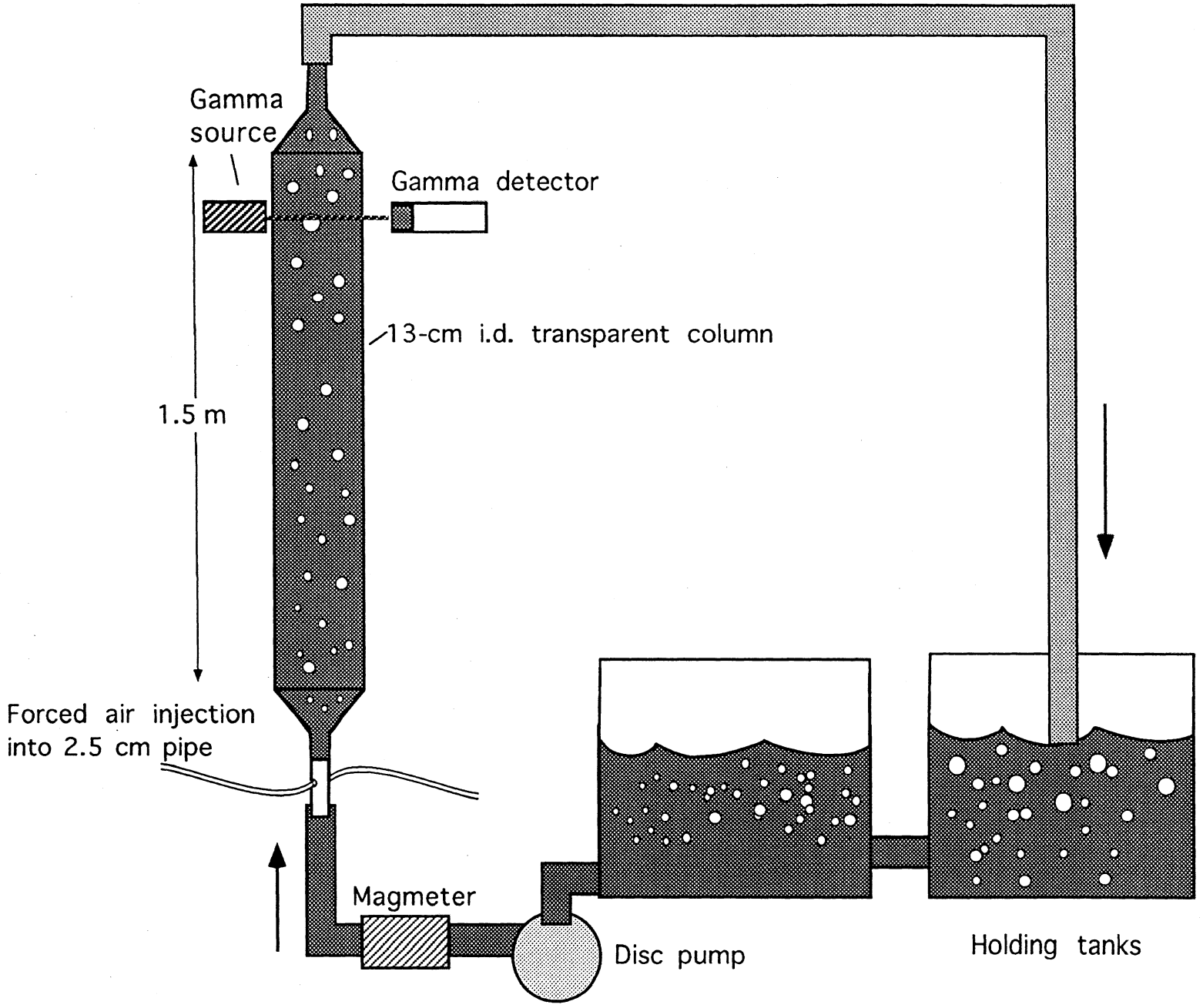

Figure 3. Cocurrent flow test facility.

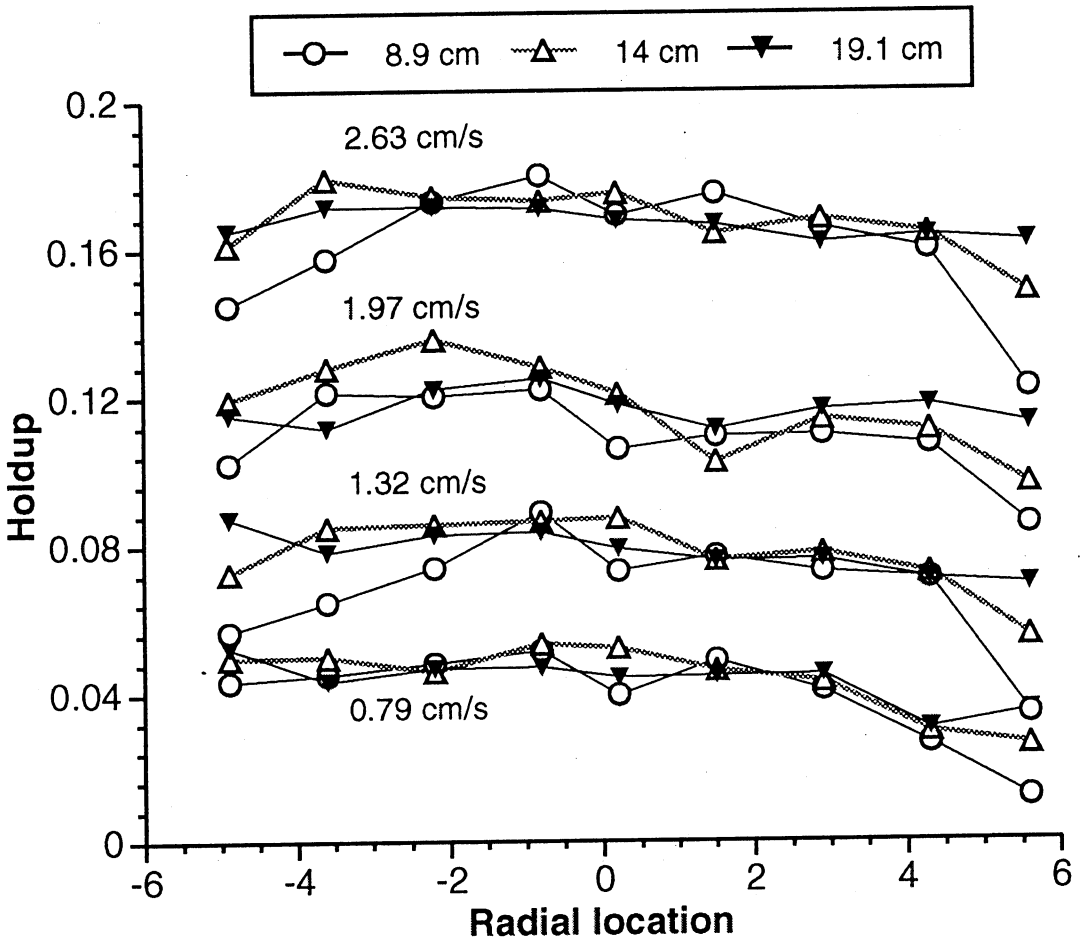

Figure 4. Chord-averaged gas holdup profiles in pure water for $j_G \leq 2.63$ cm/s, quiescent liquid apparatus.

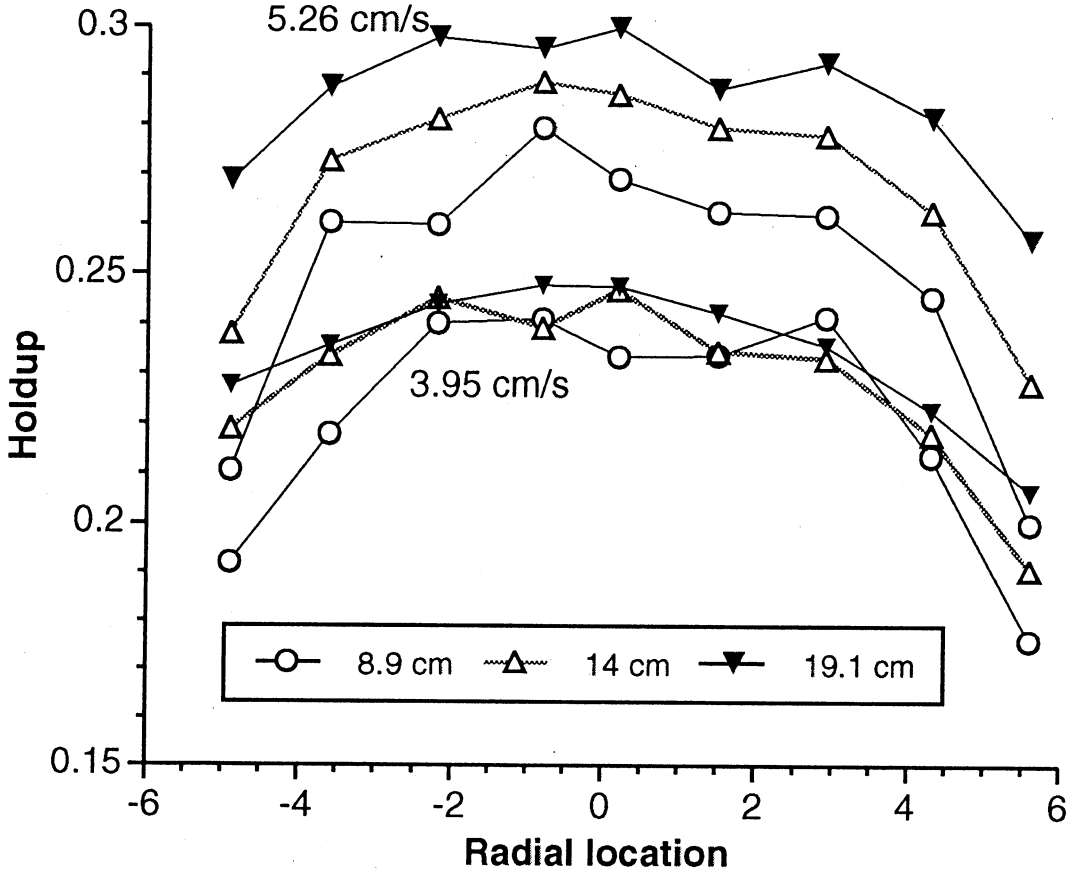

Figure 5. Chord-averaged gas holdup profiles in pure water for j_G = 3.95 and 5.26 cm/s, quiescent liquid apparatus.

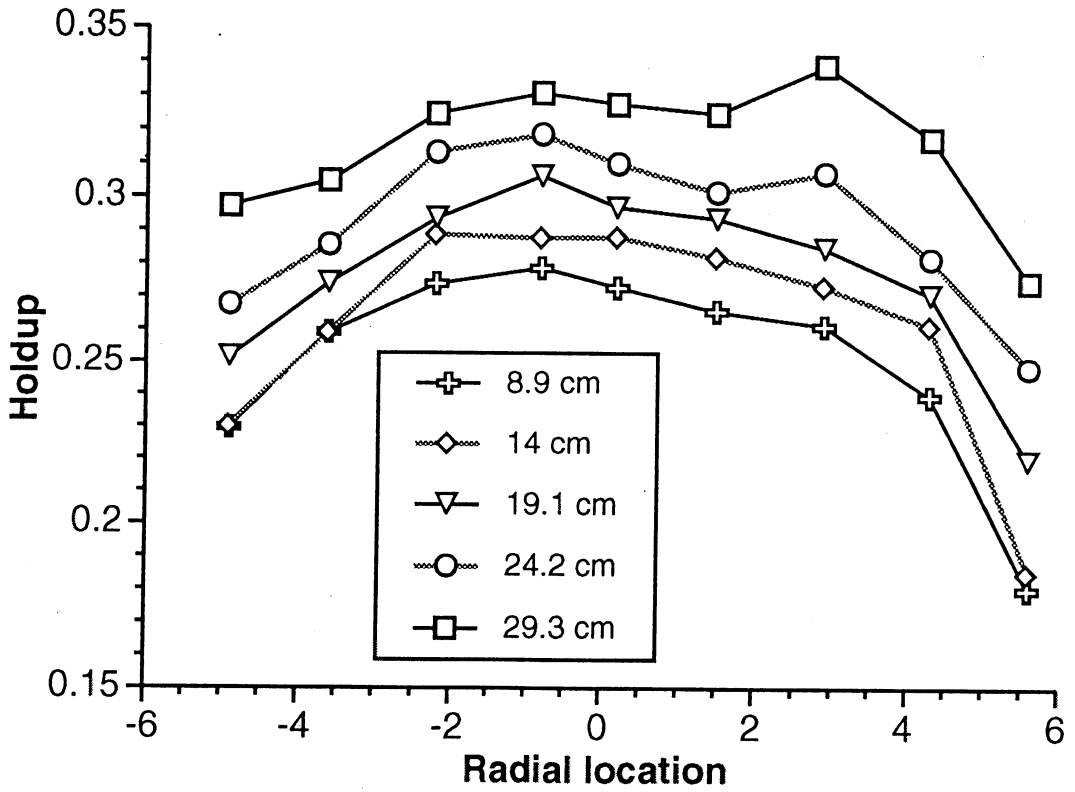

Figure 6. Chord-averaged gas holdup profiles in pure water for j_G = 6.58 cm/s, quiescent liquid apparatus.

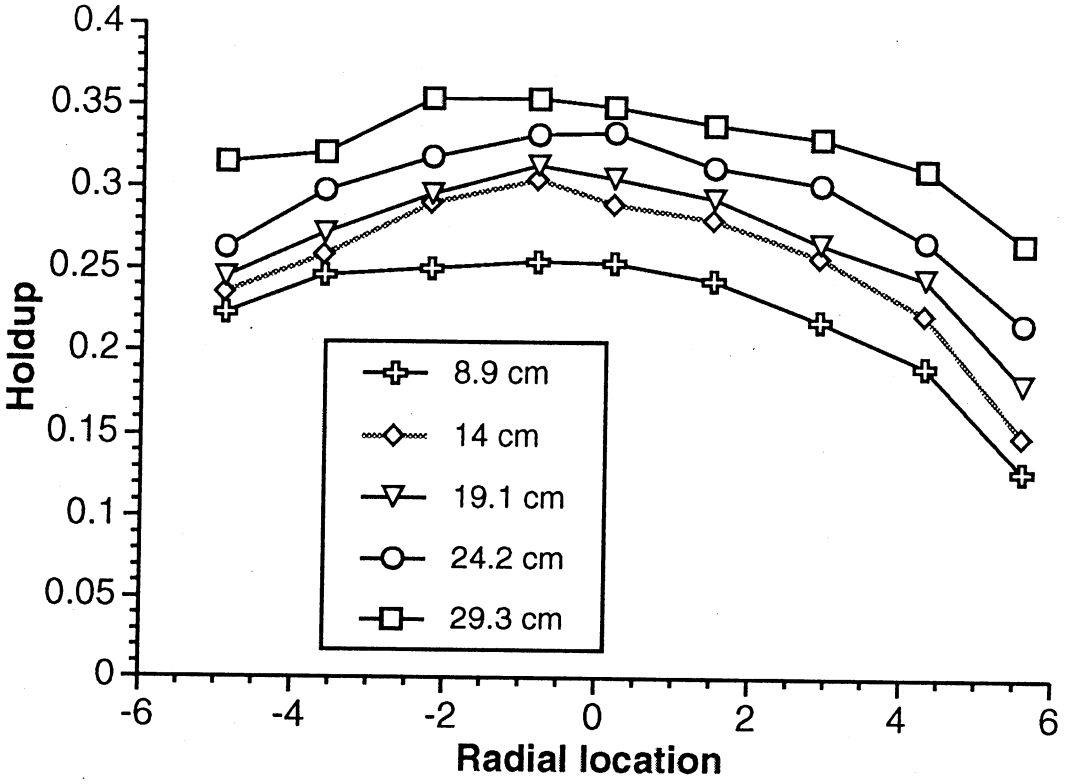

Figure 7. Chord-averaged gas holdup profiles in pure water for j_G = 9.21 cm/s, quiescent liquid apparatus.

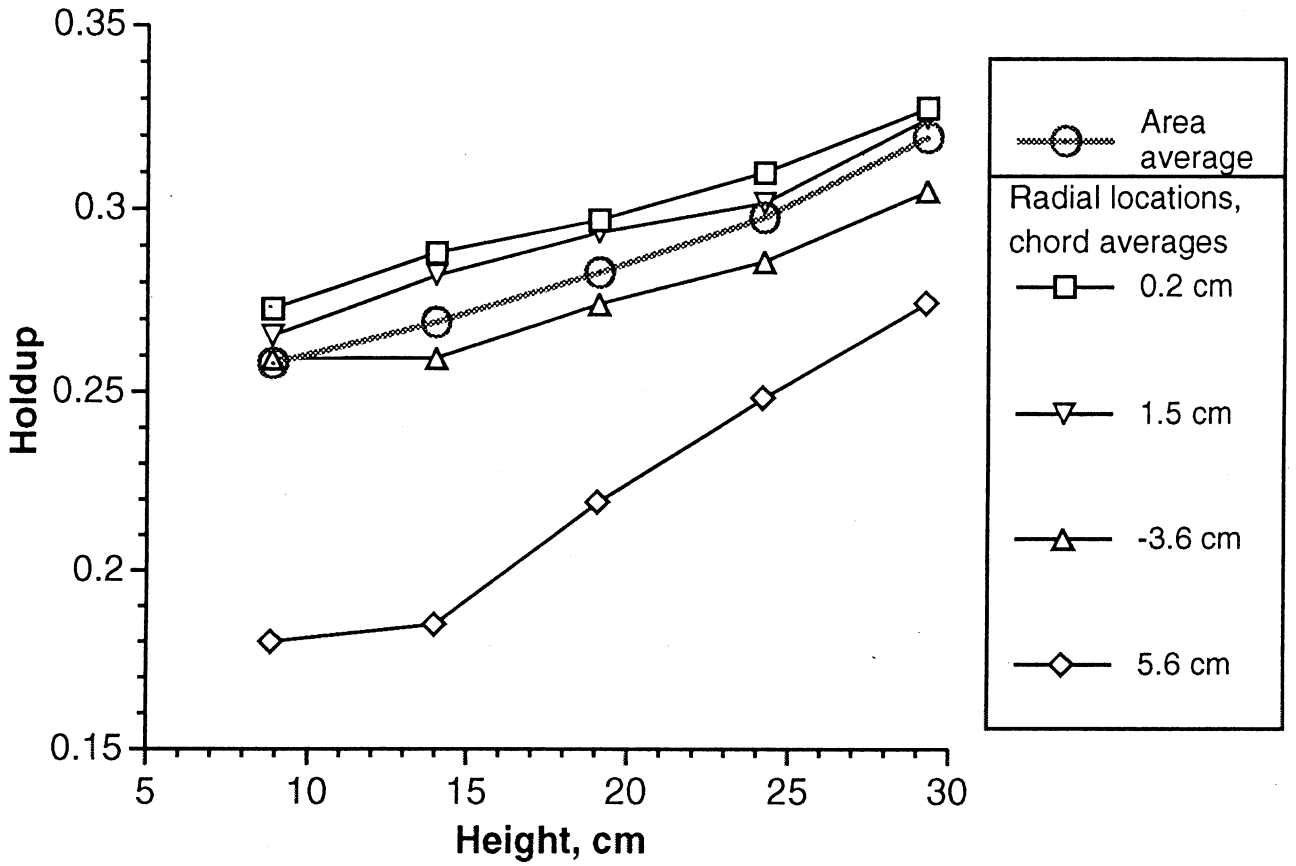

Figure 8. Gas holdup in water as a function of height for j_G = 6.58 cm/s at several chord positions, shown with cross-sectional averaged holdup.

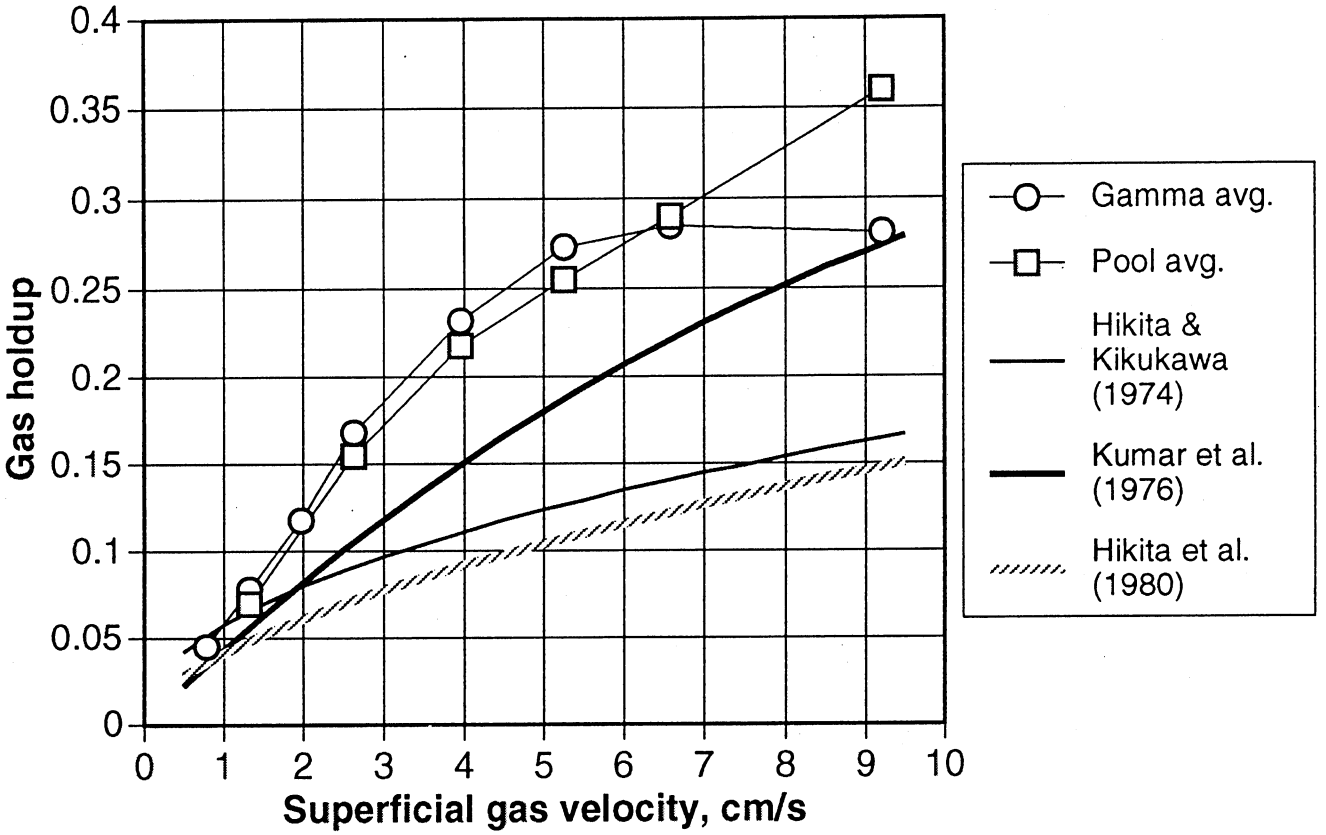

Figure 9. Comparison of literature correlations to experimental data for column averaged gas holdup in pure water. Reported data includes gamma densitometry and pool height methods.

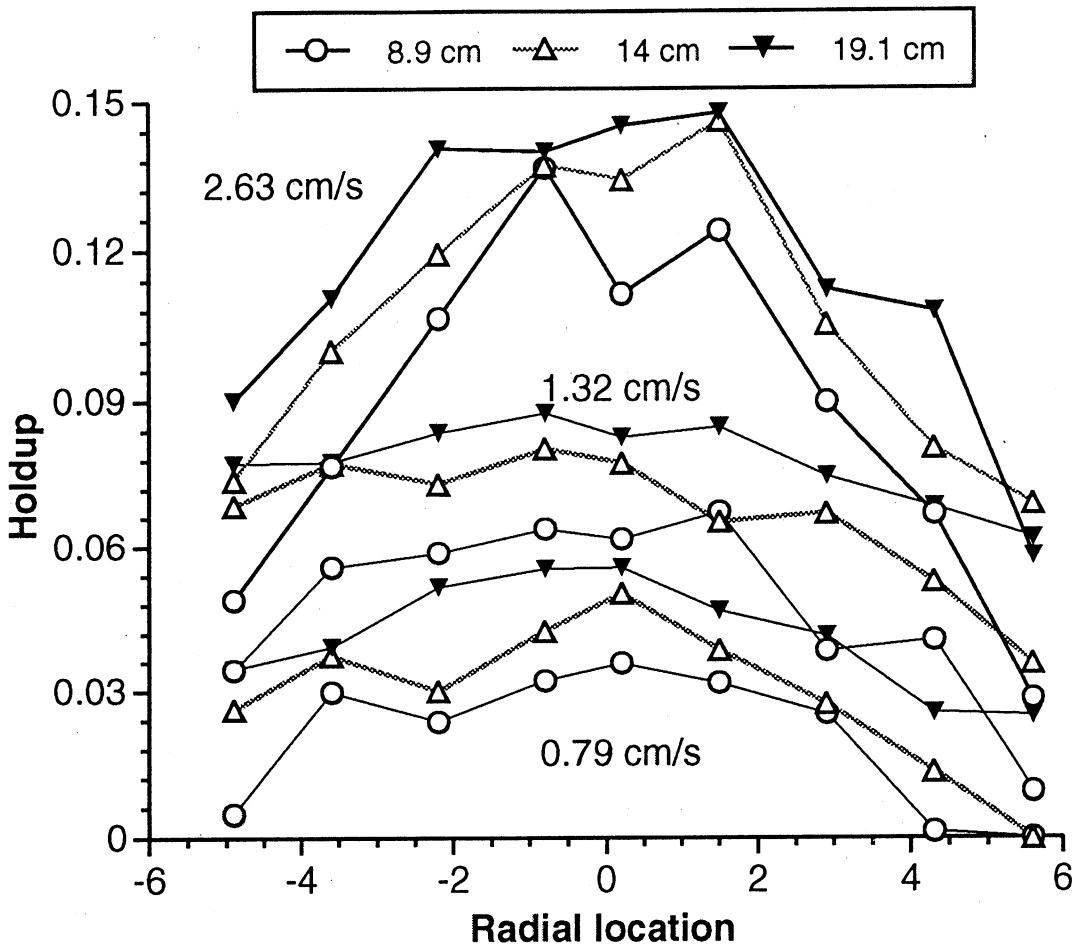

Figure 10. Chord-averaged gas holdup profiles in 1% pulp slurry for $j_G \leq 2.63$ cm/s, quiescent liquid apparatus.

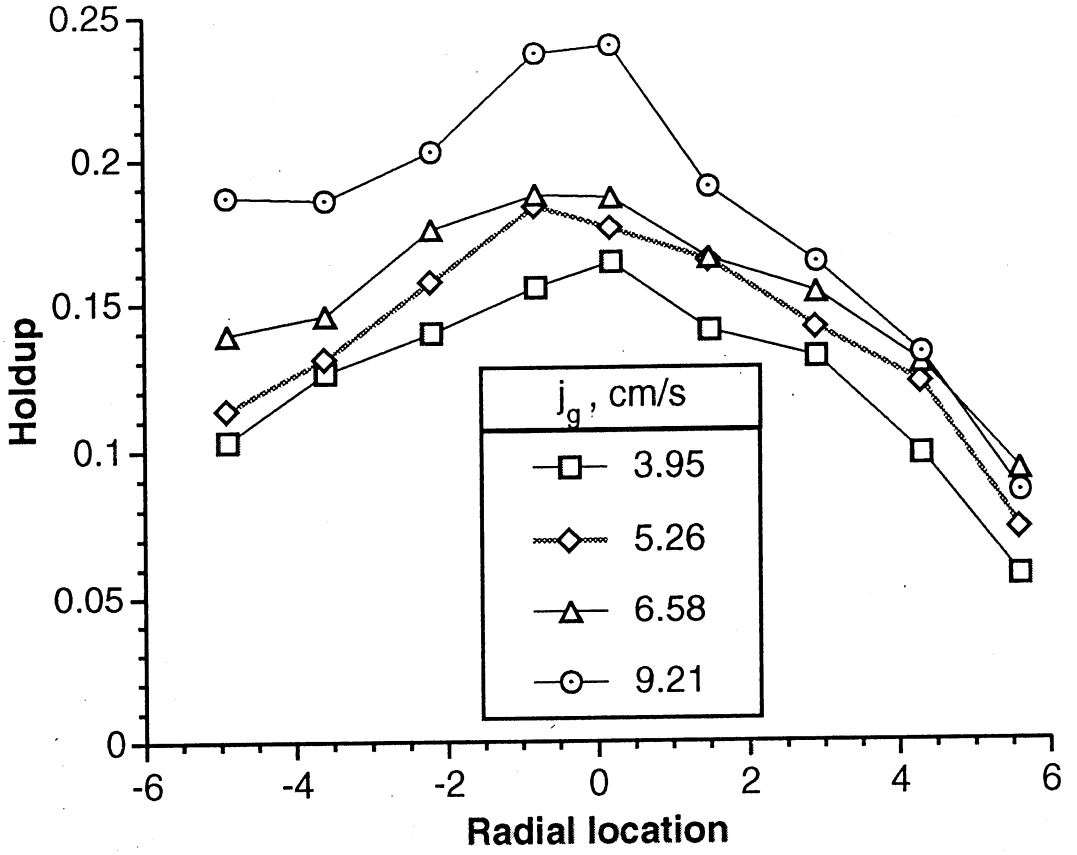

Figure 11 Chord-averaged gas holdup profiles in 1% pulp slurry at h = 19.1 cm for $j_G \geq 3.95$ cm/s, quiescent liquid apparatus.

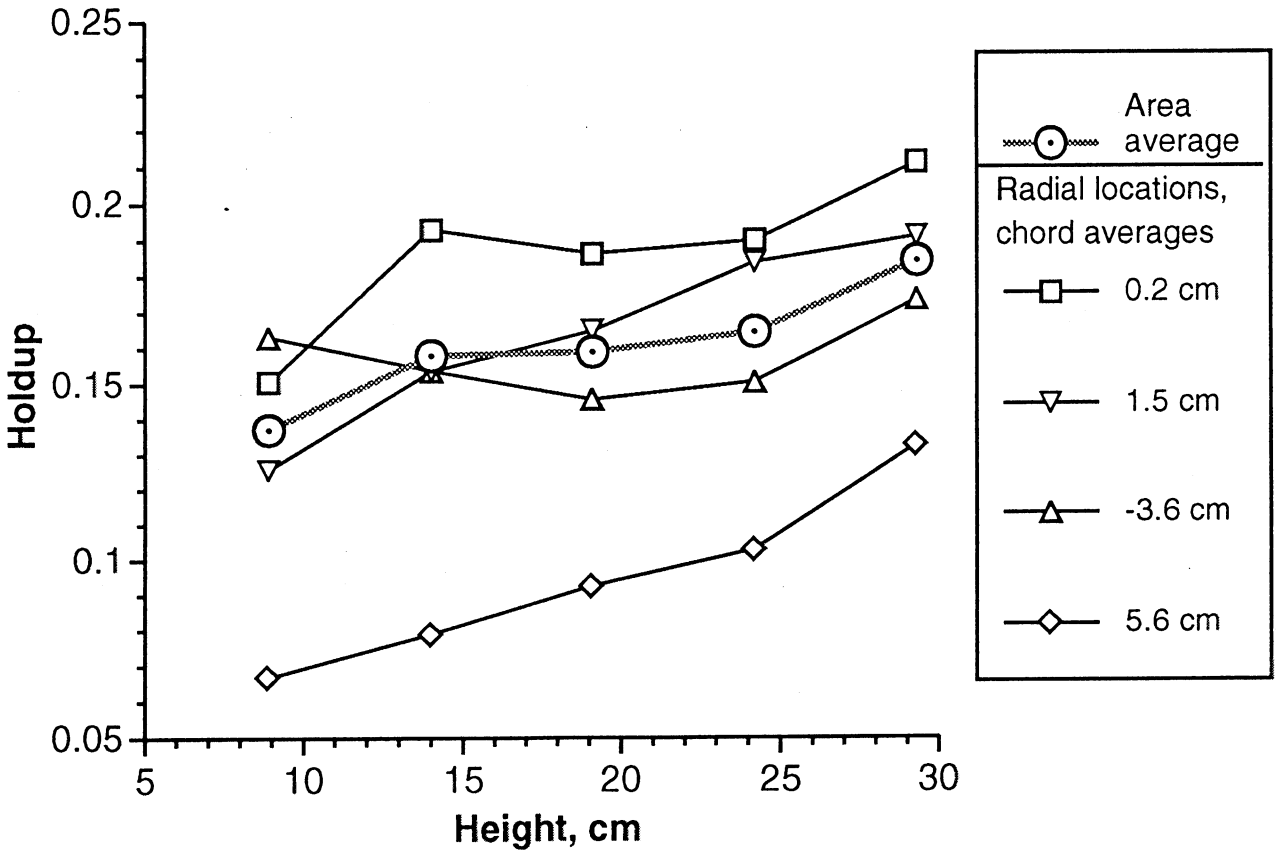

Figure 12. Gas holdup in 1% pulp as a function of height for j_G = 6.58 cm/s at several chord positions, shown with cross-sectional averaged holdup.

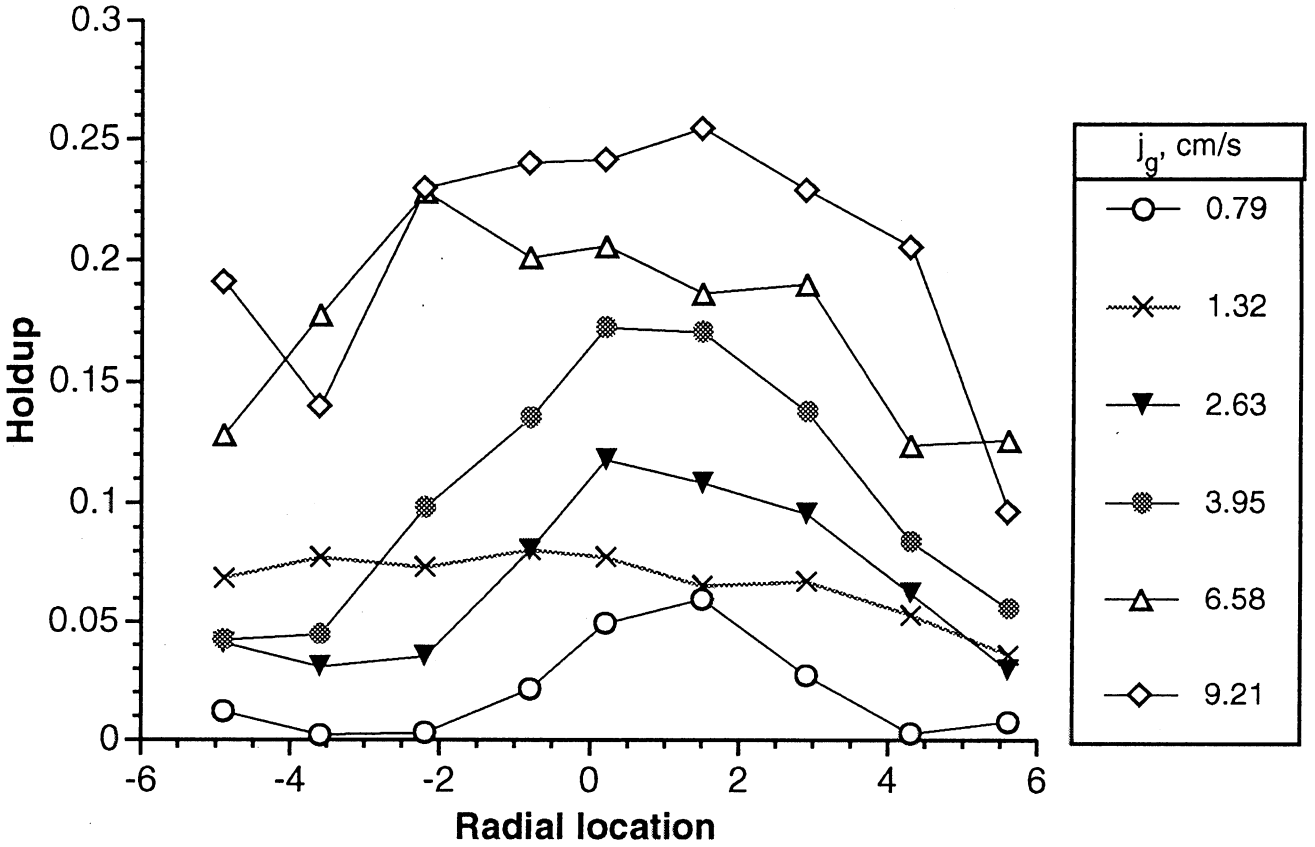

Figure 13. Chord-averaged gas holdup profiles in 2% pulp slurry at h = 19.1 cm, quiescent liquid apparatus.

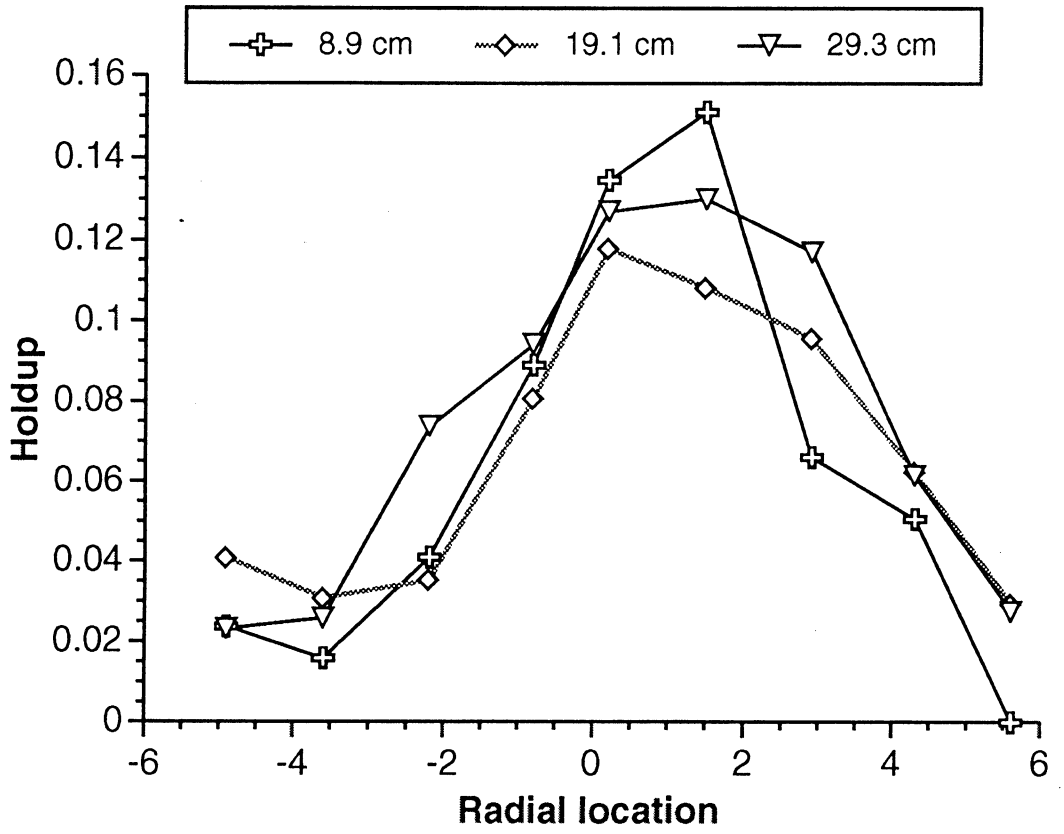

Figure 14. Selected chord-averaged gas holdup profiles in 2% pulp slurry for j_G = 2.63 cm/s, quiescent liquid apparatus.

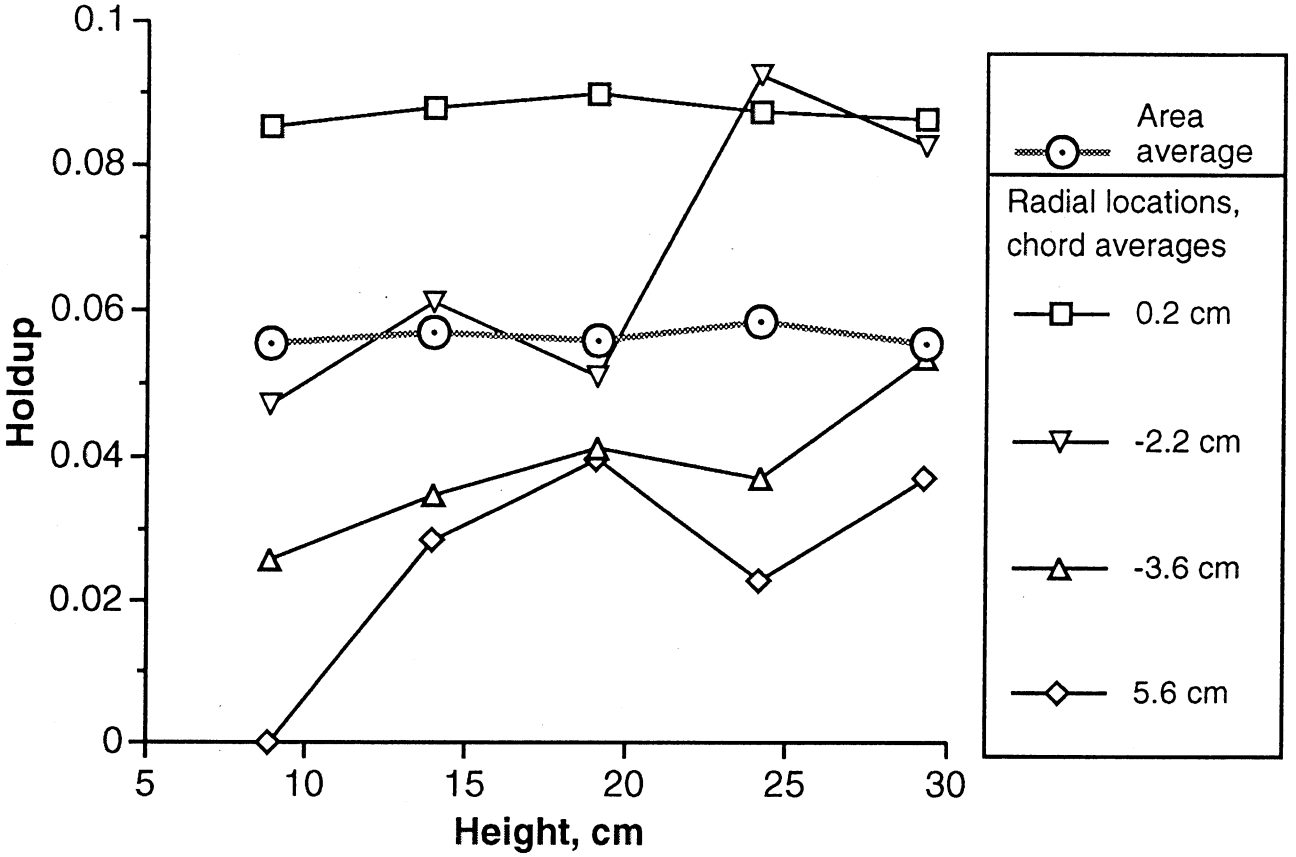

Figure 15. Gas holdup in 2% pulp as a function of height for j_G =1.97 cm/s at several chord positions, shown with cross-sectional averaged holdup.

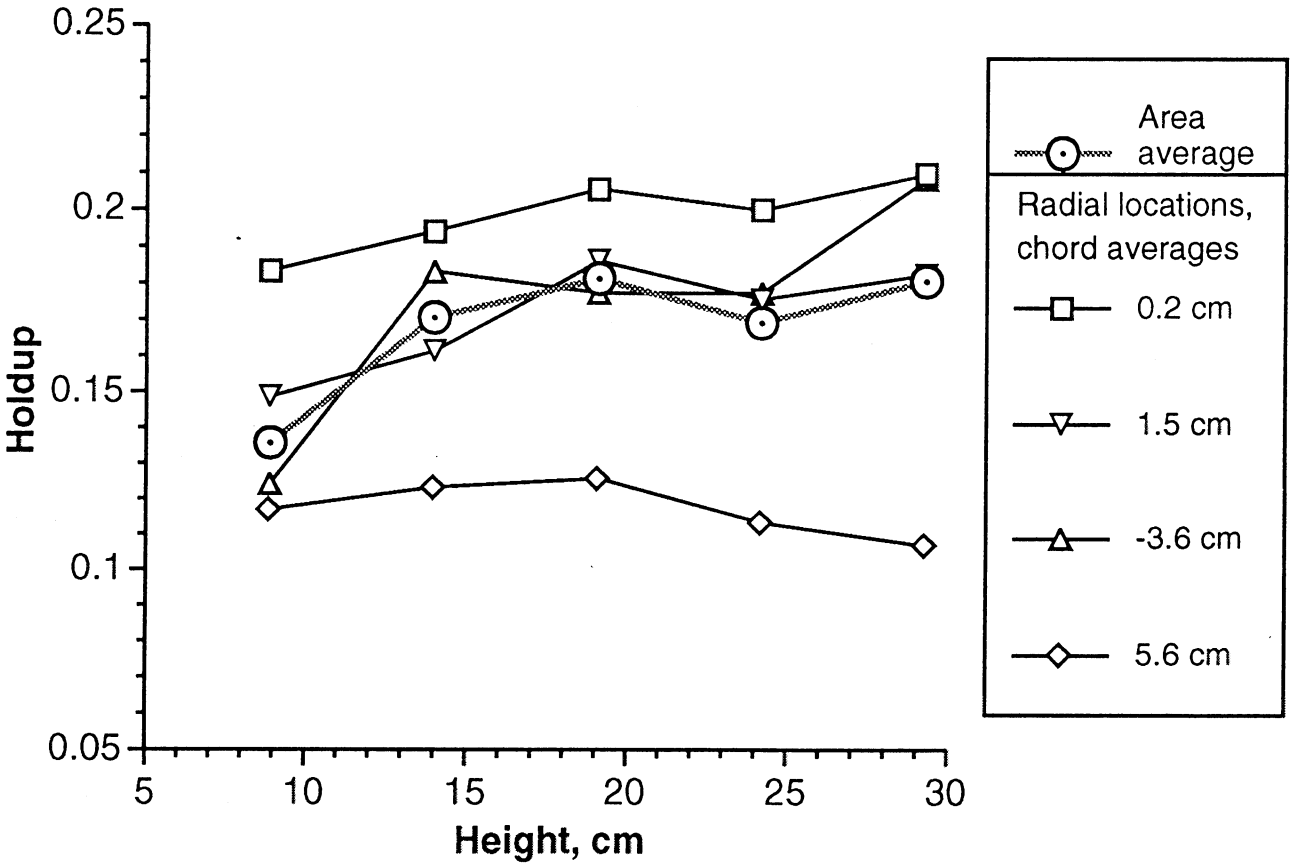

Figure 16. Gas holdup in 2% pulp as a function of height for j_G = 6.58 cm/s at several chord positions, shown with cross-sectional averaged holdup.

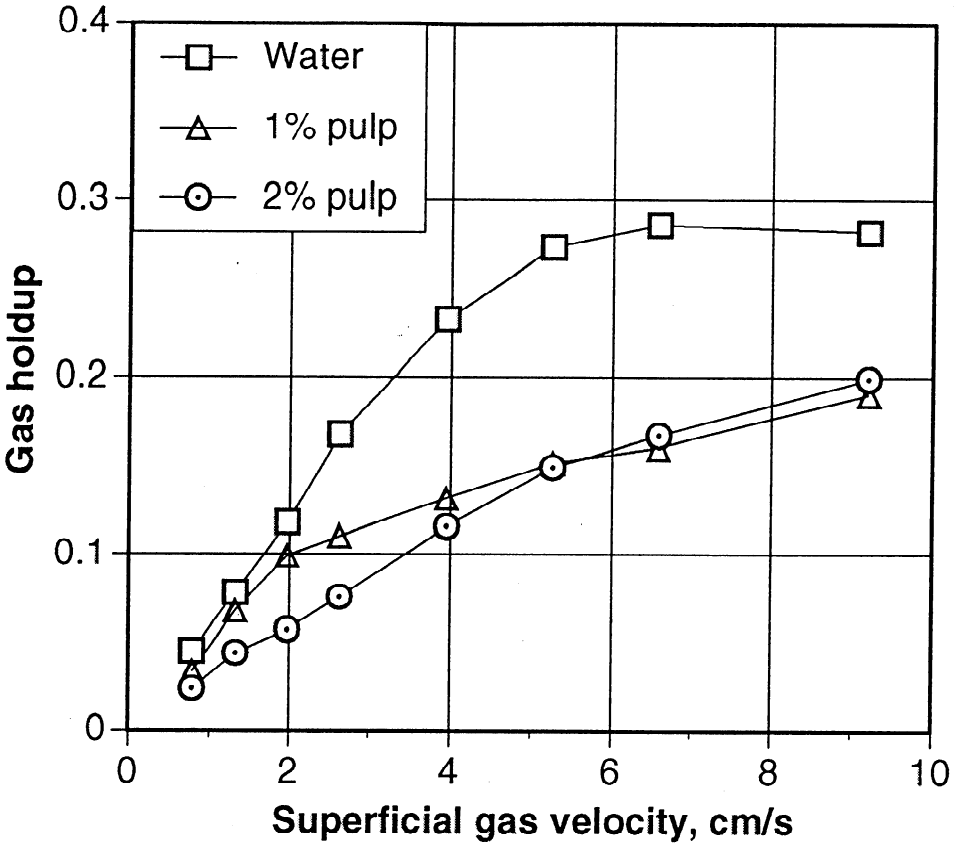

Figure 17. Column averaged gas holdup values based on gamma densitometry for water and pulp as a function of superficial gas velocity.

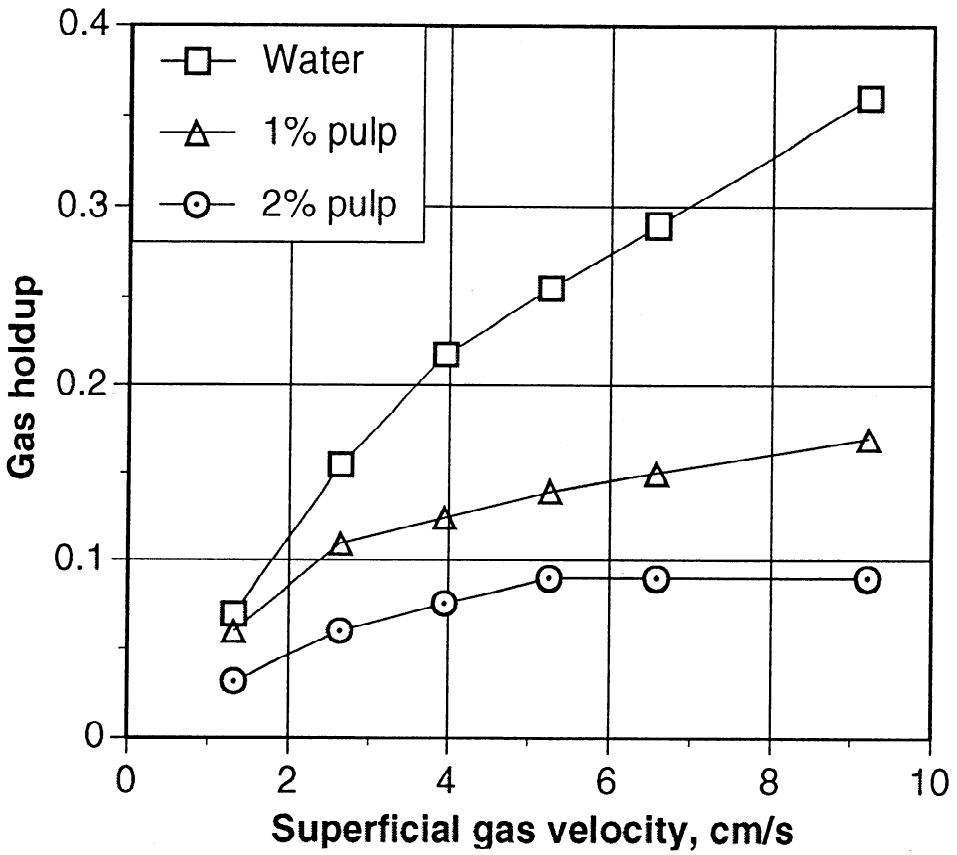

Figure 18. Column averaged gas holdup values based on pool height change for water and pulp as a function of superficial gas velocity.

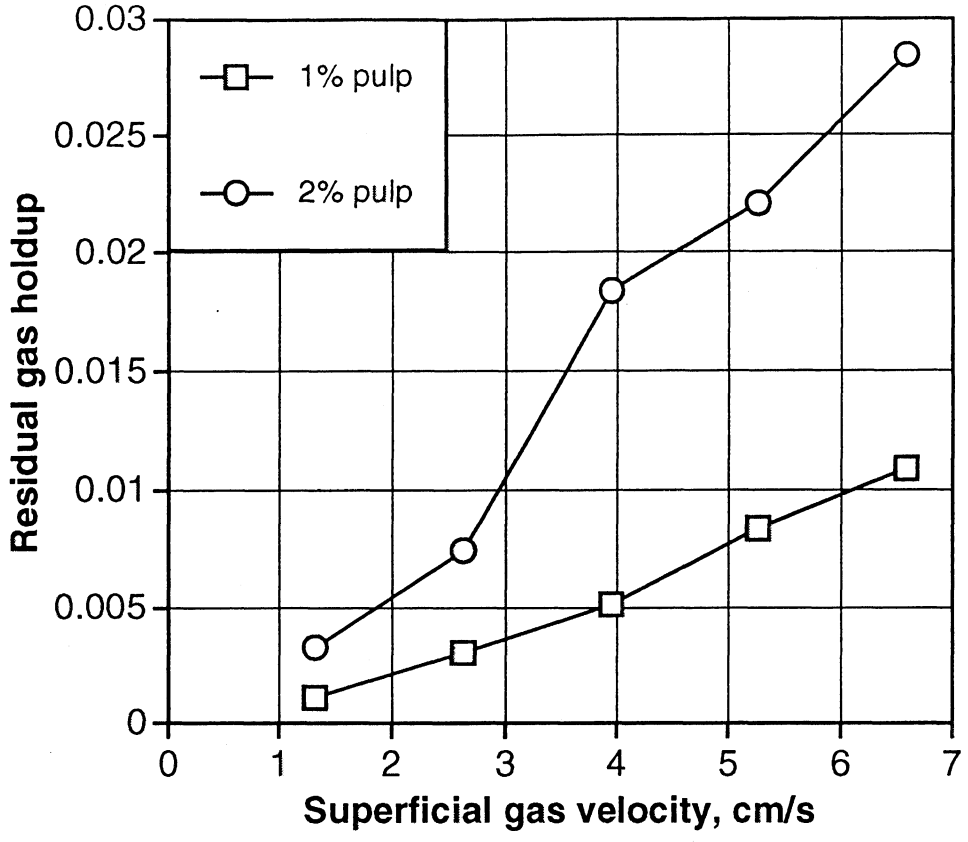

Figure 19. Residual gas holdup values averaged over the cross section of Plane h2 (19.1 cm elevation) for 1% and 2% pulp.

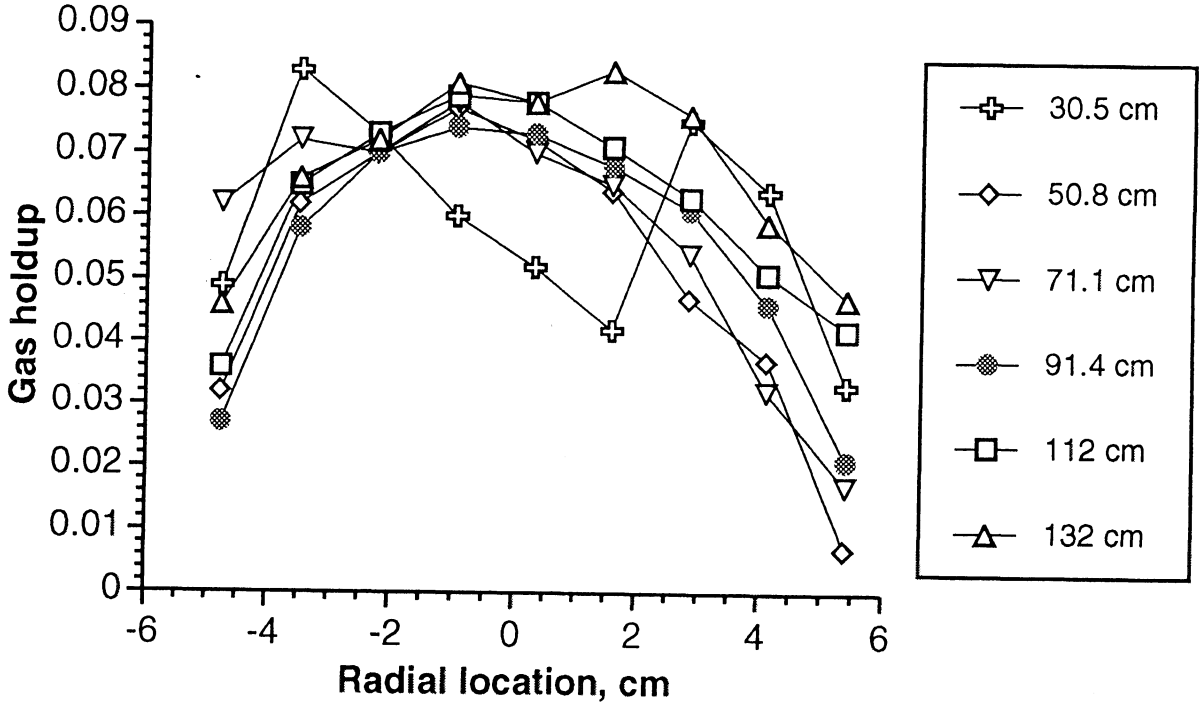

Figure 20. Chord-averaged gas holdup profiles for water in the cocurrent flow column with a liquid flux of 2.5 cm/s and a gas flux of 2.1 cm/s.

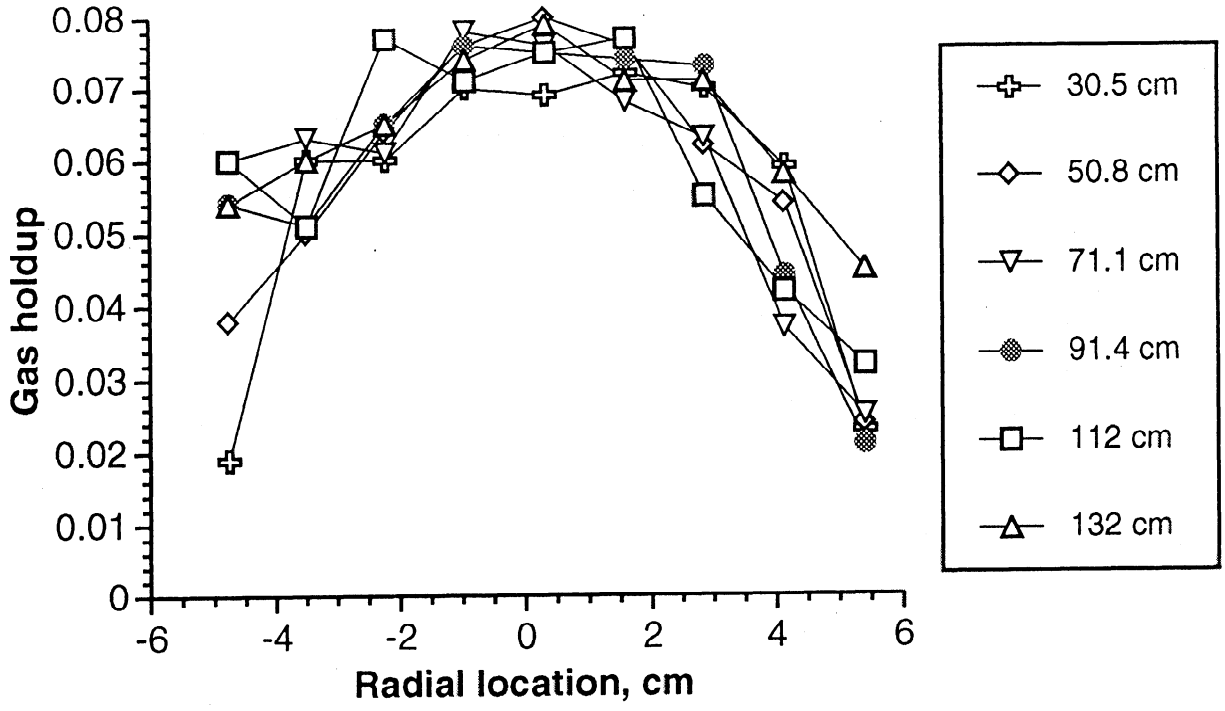

Figure 21. Chord-averaged gas holdup profiles for water in the cocurrent flow column with a liquid flux of 5 cm/s and a gas flux of 2.1 cm/s.

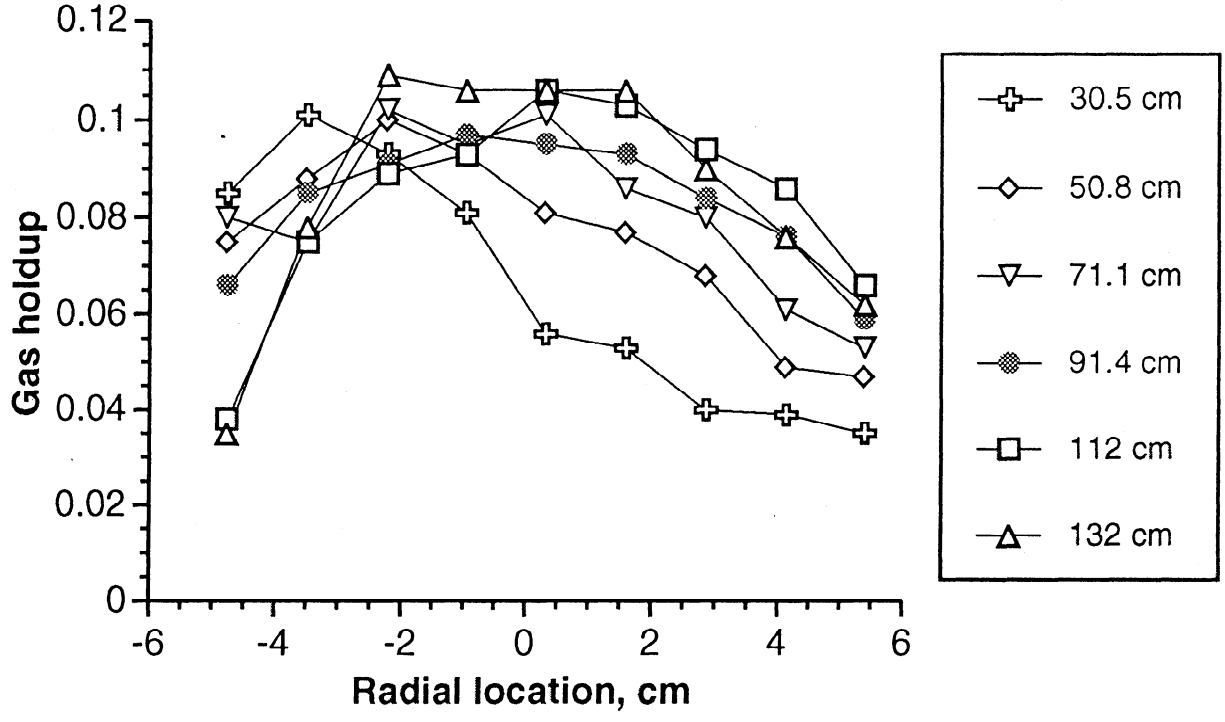

Figure 22. Chord-averaged gas holdup profiles for 1% pulp in the cocurrent flow column with a liquid flux of 2.5 cm/s and a gas flux of 2.1 cm/s.

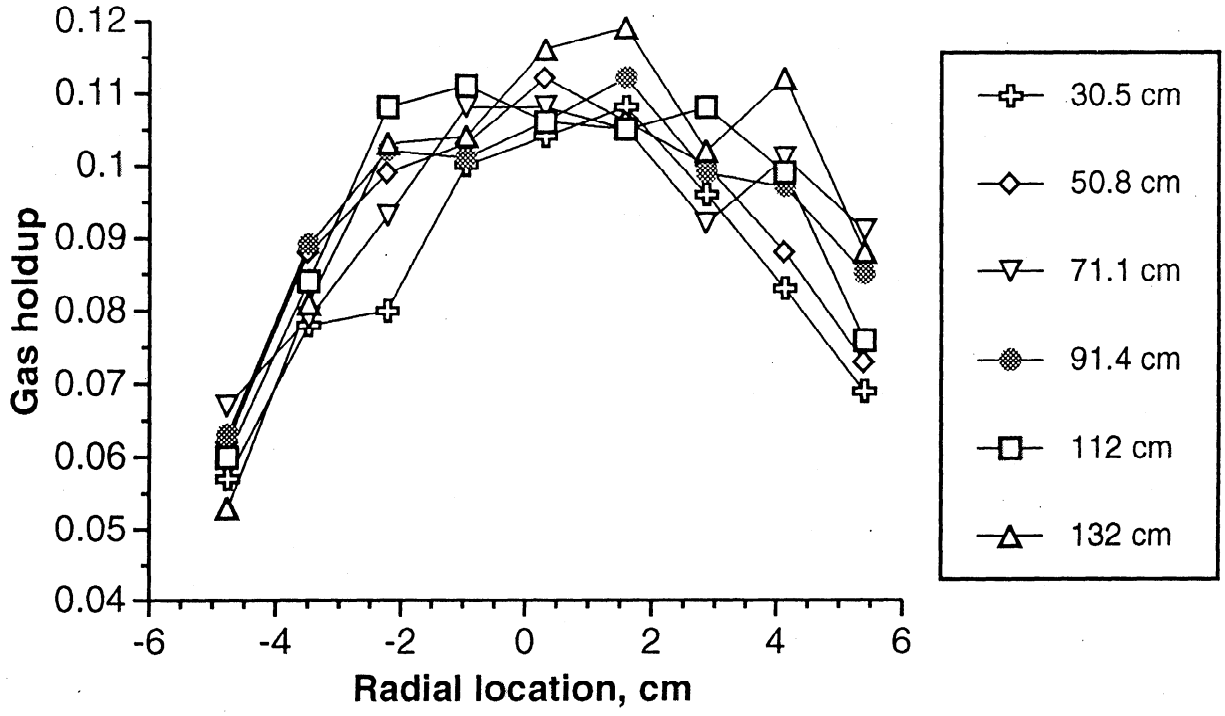

Figure 23. Chord-averaged gas holdup profiles for 1% pulp in the cocurrent flow column with a liquid flux of 5 cm/s and a gas flux of 2.1 cm/s.

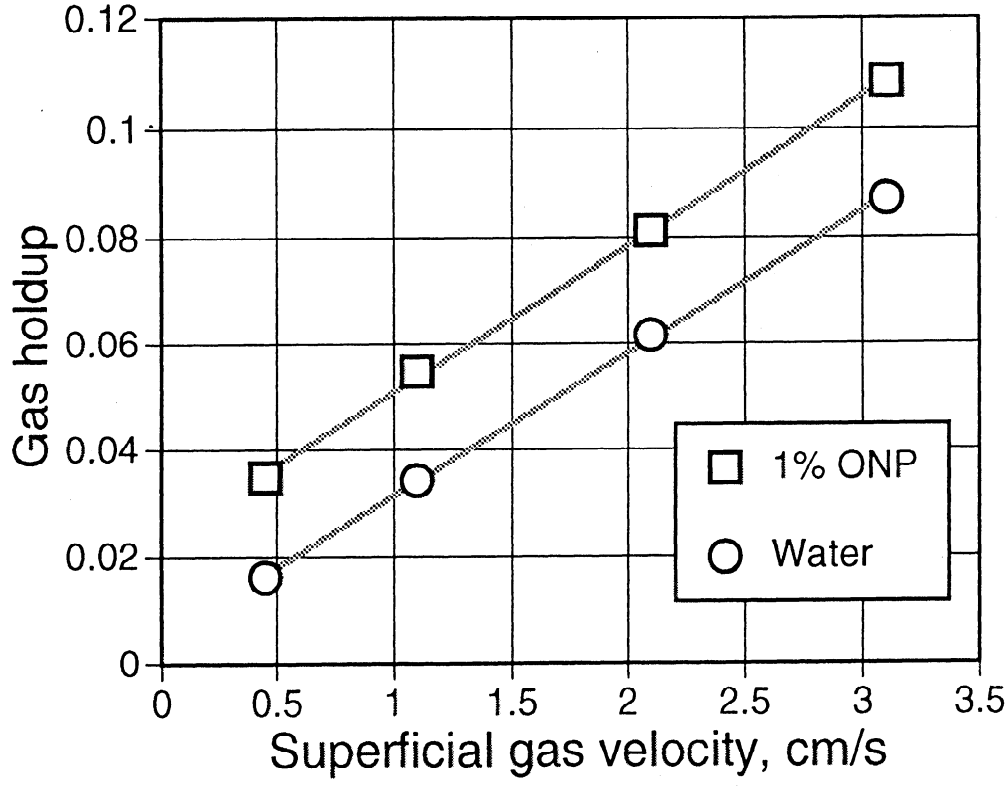

Figure 24. Column averaged gas holdup in water and 1% pulp at j_L = 2.5 cm/s.

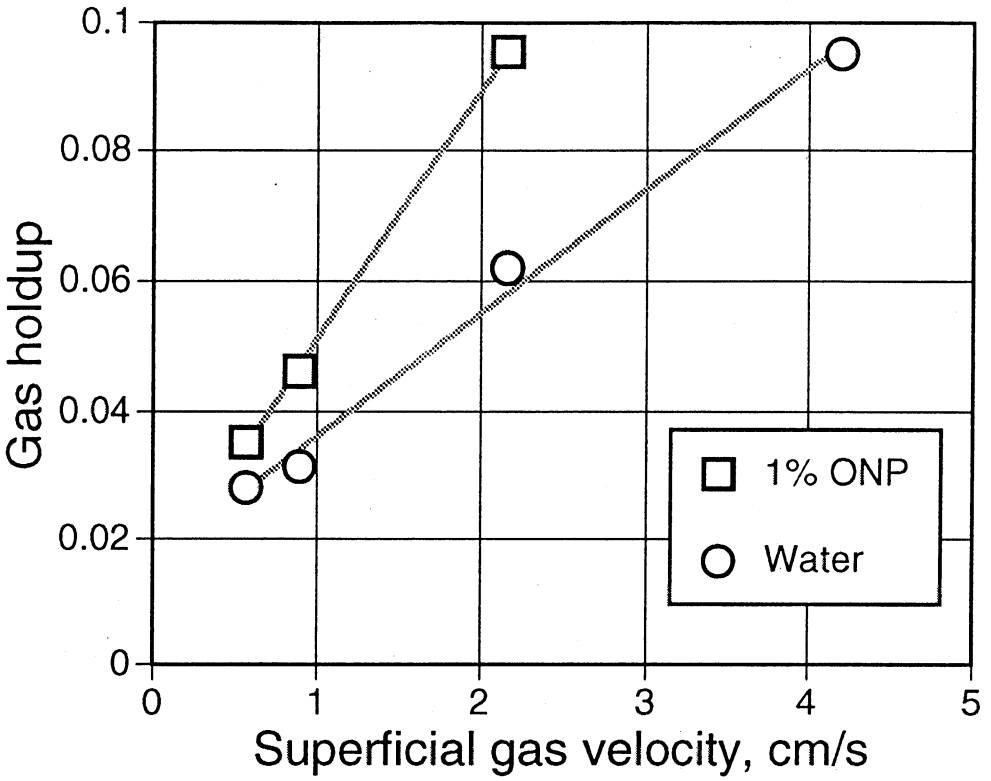

Figure 25. Column averaged gas holdup in water and 1% pulp at j_L = 5 cm/s.

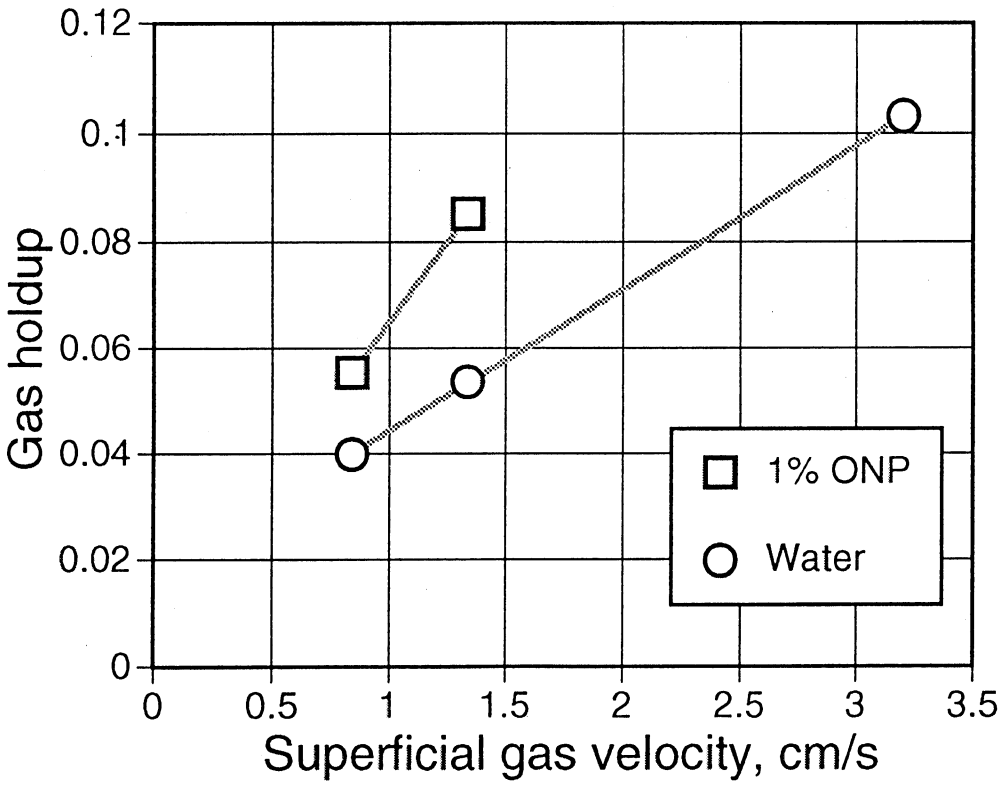

Figure 26. Column averaged gas holdup in water and 1% pulp at j_L = 7.5 cm/s.

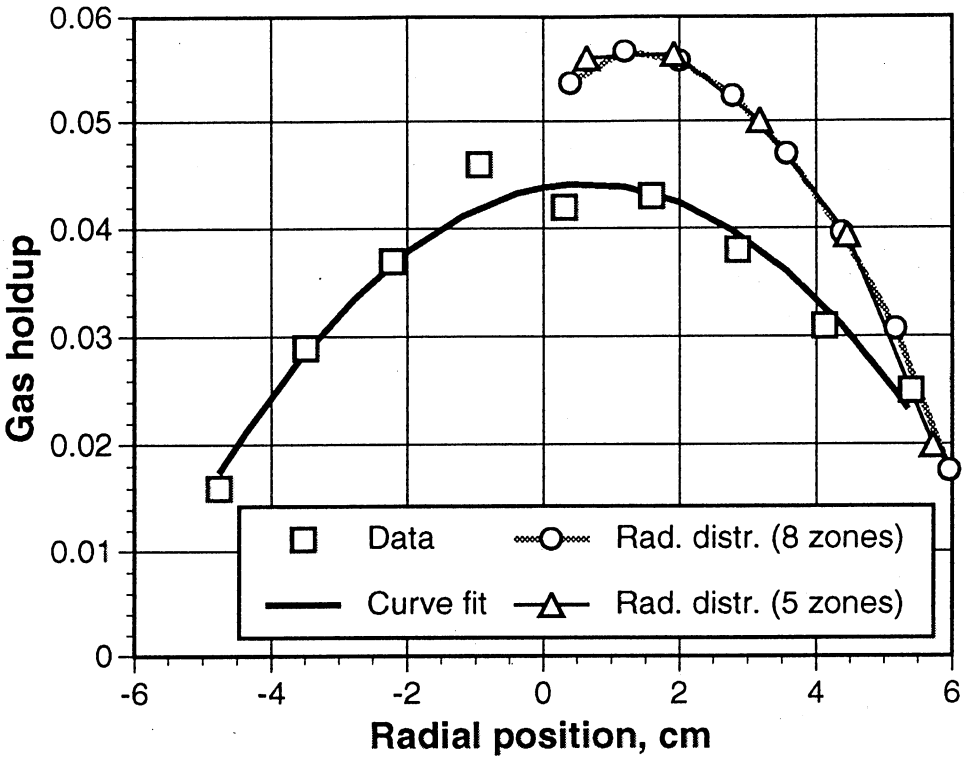

Figure 27. Comparison of raw data and computed radial gas distribution for a data set from the cocurrent flow column with 1% pulp (h=30.5 cm, j_L = 5 cm/s, j_G = 0.56 cm/s).

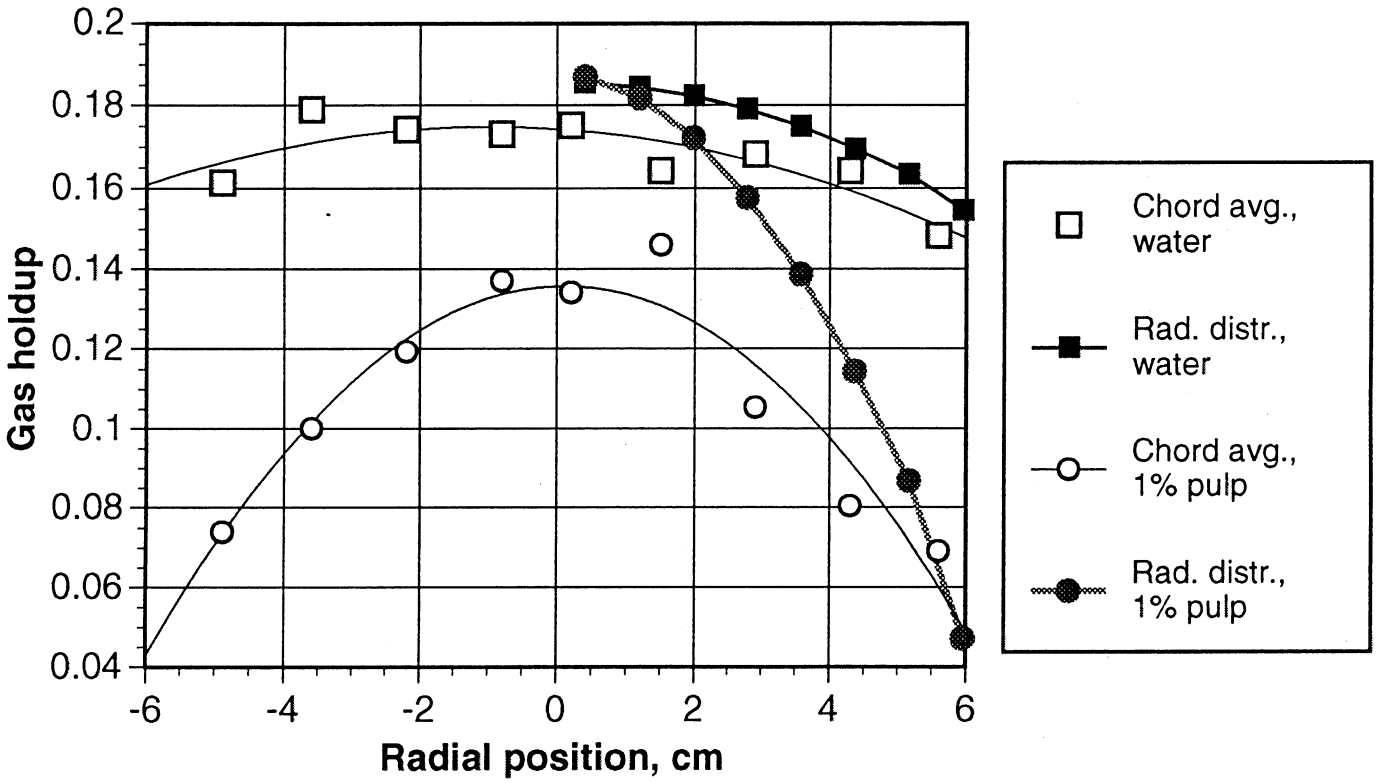

Figure 28. Chord averages and computed radial gas distributions in the quiescent flow system for both water and pulp with j_G = 2.63 cm/s at an elevation of 19.1 cm.

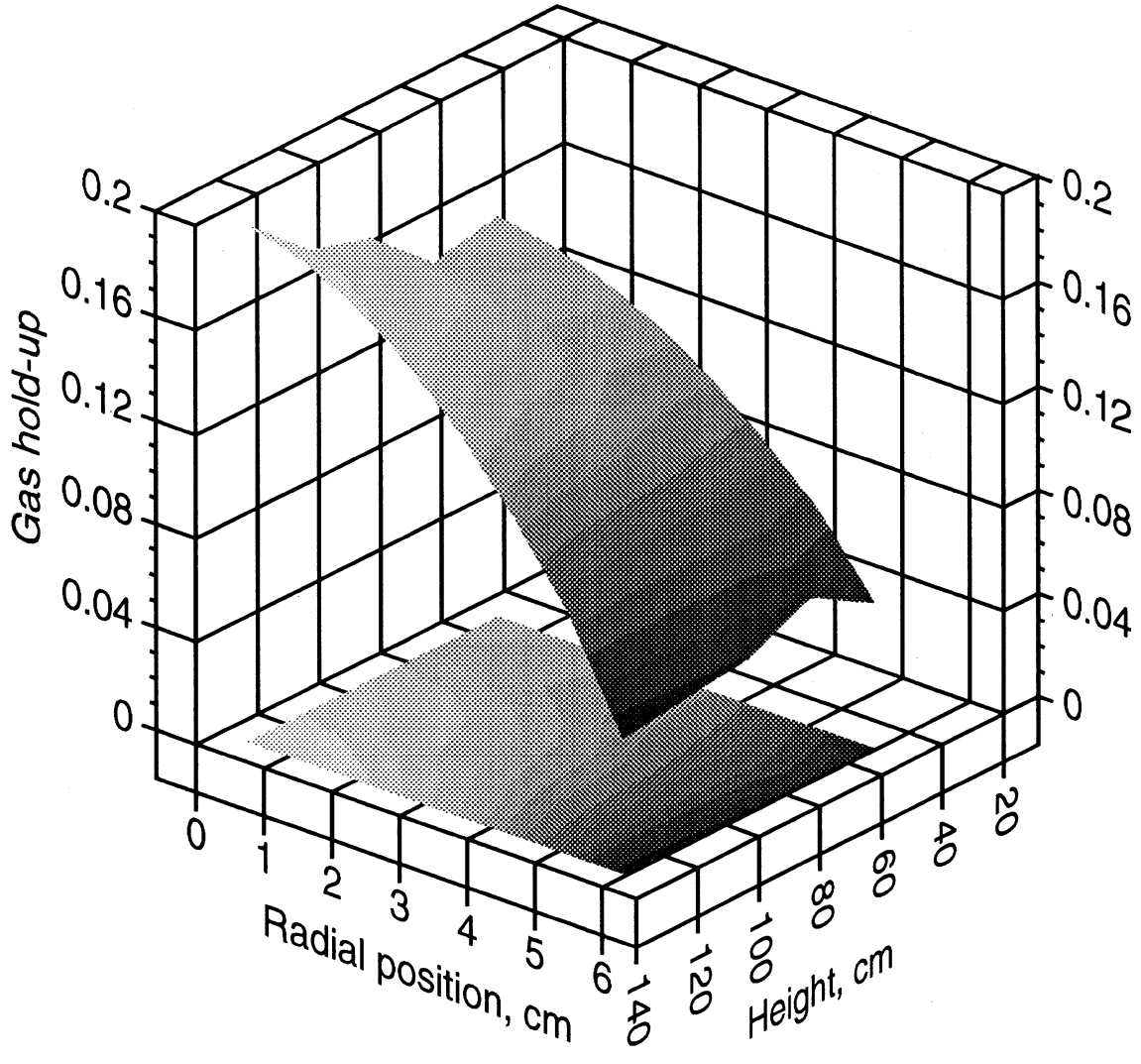

Figure 29. Computed axisymmetric gas holdup values throughout the cocurrent flow column for 1% pulp with j_L = 2.5 cm/s and j_G = 3.1 cm/s.